Argonaute-mediated cytoplasmic lattice-assembling as a ubiquitin-safebox for proteostasis stiffness in oocytes

Junchao Xue[1,2,3,#], Shuxian Liu[1,2,3,#], Lidan Xu[1,2,3,#], Yuru Luo[1,2,3], Yan Zhang[1,2,3], Bailun Li[2,3], Zhenzhen Li[1,2,3], and En-Zhi Shen[1,2,3,4,✉].

Affiliations

[1]Key Laboratory of Growth Regulation and Translational Research of Zhejiang Province, School of Life Sciences, Westlake University, Hangzhou, Zhejiang, China.

[2]Westlake Laboratory of Life Sciences and Biomedicine, Hangzhou, Zhejiang, China.

[3]Institute of Biology, Westlake Institute for Advanced Study, Hangzhou, Zhejiang, China.

[4]State Key Laboratory of Gene Expression, School of Life Sciences, Westlake University, Hangzhou, Zhejiang, China.

✉To whom correspondence should be addressed: shenenzhi@westlake.edu.cn (E.S.).

[#] These authors contributed equally to this work.

Abstract

Oocytes are exceptionally long-lived cells and need to accumulate substantial cytoplasm during growth to support early embryonic development. Over their extended lifespan, protein degradation poses a constant threat to intracellular homeostasis, yet the protective mechanisms counteracting degradation remain poorly understood. Here we show that the oocyte-specific fibrous structure, cytoplasmic lattices (CPLs), functions as a tandem ubiquitin "safebox" that shields maternal proteins from ubiquitin-mediated proteolysis. By sequestering key soluble ubiquitin-conjugating enzymes and ubiquitin ligases within their highly stable architecture, assembled CPLs enable long-term suppression of K48-linked ubiquitination. We identify Argonaute AGO2 as a critical regulator of CPL assembly: by inhibiting proteasome activity, AGO2 allows efficient accumulation of CPL components during early assembly stages, thereby promoting the formation of a fully assembled, proteasome-resistant CPL structure. Integrated proteomic and functional analyses reveal that the release of four ubiquitination regulators—previously sequestered within CPLs—underlies maternal protein remodeling and early embryonic arrest upon CPL disassembly. Together, Argonaute-mediated CPL assembly represents a novel ubiquitin-suppressive strategy. We speculate that the exceptional stability of CPL precisely provides a crucial safeguard for maintaining robust protein homeostasis in oocytes during their prolonged life.

Introduction

In most mammals, oocytes are among the longest-lived cells. They require weeks to months to grow and mature into fertilizable eggs[1-4]. During this prolonged phase, oocytes gradually increase in size and accumulate a substantial reservoir of maternal proteins[3-5]. Upon fertilization, these maternal proteins are delivered to the zygote to support early embryonic development[4,6]—a crucial strategy given the limited transcriptional and translational activity in the early embryo[7,8]. While the benefits of this maternal provisioning are evident, a key requirement for its success is the faithful preservation of homeostatic proteins within oocyte. Nevertheless, how oocytes maintain long-term proteostasis throughout their extended lifespan to preserve their developmental potential is largely unknown.

As proteostasis is essential for maintaining proper cellular function[9-11], specialized mechanisms likely exist in oocytes to establish their standing proteostatic regulation. At the core of proteostasis lies the ubiquitin-proteasome system (UPS)[10,12], which mediates the degradation of soluble ubiquitinated proteins[13]. Ubiquitination plays a critical role in oocyte growth[14,15] and meiotic maturation[14,16,17], and proteasome activity has been implicated in both oocyte maturation[1] and early embryonic development[18] across various species. How the activities of ubiquitination and proteasome are regulated during oocyte development remains poorly understood.

CPLs were first discovered by electron microscopy in the 1960s as abundant fibrous structures that occupy nearly 10% of the oocyte cytoplasm, implying a substantial and indispensable function in oocyte biology[19-21]. Several studies revealed that CPL assembly depends on oocyte-specific proteins—PADI6 and components of the subcortical maternal complex (SCMC), including MATER, TLE6, FILIA, NLRP4f, and ZBED3—and loss of any of these proteins disrupts CPL formation, causes degradation of maternal proteins[21], and results in embryonic arrest after fertilization[22-24]. Based on these observations, it has been assumed that CPLs serve as a structural scaffold for the direct storage of maternal proteins, enabling their rapid deployment upon fertilization[21]. This assumption is surprising because CPLs persist from the oocyte stage through the early embryonic cleavage stages up to the 8-cell embryo[21], and cryo-electron tomography analyses have not revealed enrichment of protein cargo along

CPL fibers[21]. Moreover, our recent work has dissected the molecular basis of CPL assembly, revealing that they are formed by 14 distinct proteins and show no evidence of bound protein cargo[25]. Taken together, these findings prompted us to investigate how CPLs regulate maternal protein preservation.

Results

Developmental assembly of CPL during oocyte growth and meiotic maturation

CPLs are abundant in fully grown oocytes (FGO) and metaphase II (MII) oocytes[21,26,27], but their developmental dynamics remain poorly defined **(Fig. 1a)**. To characterize CPL assembly during oocyte growth and meiotic maturation, we analyzed mouse oocytes across stages using transmission electron microscopy (TEM). CPLs were undetectable in secondary follicle (SF)-stage oocytes **(Fig. 1b, c)**. As oocytes initiated growth, CPL structures became visible in the cytoplasm of growing oocytes (GO) and were widely distributed by FGO stage. Upon meiotic resumption, CPL abundance increased further, peaking at metaphase I (MI) and remaining stable through MII **(Fig. 1b, c).** Using our recently determined cryo-EM structure of the CPL, we re-present its molecular architecture as a periodic assembly of 14 constitutive protein subunits arranged into repeating structural modules—a “U-shaped basket” (UB) and an “adapter ring” (AR) **(Fig. 1d)**.

We next examined the expression dynamics of the components. Most subunits were expressed at low levels in SF oocytes and exhibited distinct dynamics during oogenesis **(Fig. 1e)**. A subset, including UBE2D3, SKP1, UHRF1, FILIA, and FLOPED, gradually accumulated during oocyte growth. Others, such as TLE6, NLRP14, NLRP4f, TUBB2A/2B, and MATER, were strongly upregulated at the onset of growth in GO and remained stably expressed thereafter. In contrast, FBXW24 and PADI6 were constitutively abundant throughout development **(Fig. 1e)**. This coordinated upregulation of CPL subunits coincides with the onset of CPL assembly, suggesting that developmental control of subunit expression drives CPL biogenesis during oocyte growth.

CPL formation sequesters ubiquitination regulators in oocytes

Notably, four CPL components (UBE2D3, SKP1, UHRF1, and FBXW24) are established components of the ubiquitin–proteasome system (UPS). UHRF1, FBXW24, and SKP1 function as E3 ubiquitin ligases[28-30], while UBE2D3 is an E2 conjugating enzyme[31]; all are required for substrate ubiquitination. The identification of these essential ubiquitination regulators as integral CPL components raised the possibility that CPL assembly may spatially regulate their availability.

To test whether CPL formation affects the subcellular distribution of these proteins, we enriched CPLs from oocytes at different developmental stages (SF, FGO, and MII) by centrifugation **(Fig. 1f)**. In SF oocytes, prior to CPL assembly, all four proteins were predominantly present in the soluble cytoplasmic fraction **(Fig. 1g)**. In contrast, in FGO and MII oocytes, these proteins were nearly undetectable in the soluble fraction and instead quantitatively enriched in the CPL-containing pellet **(Fig. 1g)**. These results demonstrate that CPL assembly coincides with a complete shift in the localization of key ubiquitination regulators—from a diffusible, cytoplasmic state to stable incorporation into the insoluble CPL structure. Together with the developmental up-regulation of CPL subunits **(Fig. 1e)**, these findings indicate that CPL biogenesis drives the sequestration of multiple key ubiquitination regulators into a multimeric filamentous structure **(Fig. 1h; Supplementary video 1)**. This spatial confinement may serve as a structural mechanism for the suppression of global ubiquitination during oocyte growth.

CPL assembly limits K48-linked ubiquitination

To determine whether CPL formation regulates ubiquitination in oocytes, we first examined ubiquitin chain dynamics during oocyte development. As oocytes grew, levels of K48-linked ubiquitination, which is the canonical signal for proteasomal degradation[32], decreased markedly. In contrast, K63-linked ubiquitination, which primarily mediates nondegradative signaling[33], remained unchanged **(Fig. 2a–c; Extended data fig. 1a-c)**. This inverse correlation between CPL accumulation and K48 ubiquitin levels raised the possibility that CPL assembly

actively restricts K48-linked ubiquitination.

To test this hypothesis, we disrupted CPL formation by knocking out *Tle6*, a core component localized to the AR module and required for CPL assembly[23]. In TLE6-KO oocytes, CPLs were severely disrupted, and K48-linked ubiquitination increased dramatically compared to wild-type oocytes **(Fig. 2d-f; Extended data fig. 1d)**. Notably, the ubiquitination regulators UBE2D3, SKP1, UHRF1, and FBXW24, which are residents of the UB module and normally sequestered in the CPL pellet, were entirely redistributed to the soluble cytoplasmic fraction in TLE6-KO oocytes **(Fig. 2g)**. These results demonstrate that CPL assembly suppresses global ubiquitination by compartmentalizing key UPS components into a stable filamentous network. By restricting substrate access, the CPL acts as a protective "safebox" to constrain ubiquitin-mediated degradation during oocyte growth.

Next, to further determine whether the elevated K48-linked ubiquitination in CPL-deficient oocytes is driven by the mis-localization of CPL-associated ubiquitination regulators, we overexpressed FBXW24, SKP1, UBE2D3, and UHRF1 via mRNA microinjection into wild-type oocytes. Strikingly, overexpression of these four regulators resulted in a significant increase in K48-linked ubiquitination **(Fig. 2h, i; Extended data fig. 1e)**. SKP1 and FBXW24 are core components of the SCF (SKP1-CUL1-F-Box) E3 ubiquitin ligase complex, the largest family of E3 ligases[34,35], UHRF1 is a well-characterized E3 ligase that collaborates with the E2 enzyme to ubiquitinate substrates[28]. These results support the model that unrestricted activity of these regulators, when released from the CPL, is sufficient to drive aberrant K48-linked ubiquitination.

The structural results reveal that both classes of E3 ligases, SCF (SKP1–FBXW24) and UHRF1, are spatially confined within the UB module of CPL **(Fig. 2j-l)**. This raised the possibility that CPL incorporation may directly regulate their enzymatic activity. To test this, we reconstituted the ubiquitination machinery in vitro using purified recombinant proteins: SKP1, FBXW24, UBE2D3, UHRF1, and PADI6—a CPL scaffold protein that interacts with these regulators **(Extended data fig. 2a-h)**. Using established substrates RAD51 for SCF complexes and histone H3 for UHRF1[36,37], we confirmed that both E3 ligases efficiently catalyzed substrate ubiquitination **(Fig. 2m, n)**. Strikingly, addition of PADI6 strongly inhibited

ubiquitination by both E3 complexes. In contrast, PADI6 mutants defective in E2 or E3 binding failed to inhibit activity **(Fig. 2m, n; Extended data fig. 2i-j and 3a-c)**. Consistent with these biochemical findings, expressions of SKP1-FBXW24 or UHRF1 in HEK293 cells markedly increased cellular K48-linked ubiquitination. Co-expression of wild-type PADI6, but not its interaction-deficient mutants, suppressed this hyper-ubiquitination **(Fig. 2o, p)**.

Together, these results demonstrate that CPL assembly physically sequesters E2/E3 enzymes and functionally suppresses their catalytic activity. PADI6, as an integral component of CPL, functions as a direct inhibitor of multiple E3 ligases when incorporated into the CPL structure. This dual mechanism of spatial confinement and enzymatic repression underlies the reduction of K48-linked ubiquitination during oocyte growth.

AGO2 is required for CPL formation and subunit stability

CPLs begin to assemble at the onset of oocyte growth and persist throughout maturation, we next asked what mechanisms enable the stability of this dynamically assembled structure. In the process of investigating the roles of AGO2/endo-siRNAs in oocytes, we observed that AGO2 knockout (AGO2-KO) oocytes exhibited a severe loss of CPL structures **(Extended data fig. 4a)**, indicating the requirement of AGO2 for CPL formation. We then examined CPL formation across developmental stages in AGO2-KO oocytes. CPLs were nearly undetectable across all developmental stages in AGO2-KO oocytes, revealing that AGO2 is required for CPL assembly **(Fig. 3a, b)**.

To determine how AGO2 regulates CPL formation, we measured the mRNA and protein levels of CPL components in AGO2-KO oocytes. Although mRNA levels remained unchanged, nine CPL component proteins showed markedly reduced abundance in AGO2-KO oocytes **(Fig. 3c; Extended data fig. 4b)**, suggesting that AGO2 helps maintain protein stability rather than the transcription levels of CPL components.

Proteostasis in oocytes is maintained by two major degradation pathways: the ubiquitin-proteasome system and the autophagy-lysosomal pathway. To assess their activities in AGO2-KO oocytes, we first performed live staining with a fluorescent proteasome activity reporter

Me4Bodipy[38] and a lysosomal marker LysoTracker[38]. Strikingly, proteasome activity was significantly elevated in AGO2-KO oocytes, whereas lysosomal activity remained unchanged **(Fig. 3d; Extended data fig. 4c)**. To determine whether CPL components are direct targets of ubiquitin-mediated degradation, we next enriched ubiquitinated proteins using tandem ubiquitin binding entities (TUBE) beads. Immunoblotting and IP–mass spectrometry revealed robust ubiquitination of multiple CPL proteins, including NLRP4f, TLE6, and NLRP14 **(Fig. 3e, f; Extended data fig. 4d-f)**. To further test the functional consequence of these modifications, we performed protein stability assays in HEK293 cells. Mutation of the ubiquitination sites in NLRP4f, TLE6, and NLRP14 significantly blocked their degradation and increased the protein stability **(Fig. 3g, h; Extended data fig. 4g-i)**, confirming that these CPL components are regulated by ubiquitin-dependent proteasomal degradation.

AGO2 regulates CPL assembly by restricting proteasome through its slicer activity

We therefore asked whether AGO2 regulates CPL formation through suppressing proteasome activity. Treatment of AGO2-KO oocytes with proteasome inhibitors (MG132 or Bortezomib)[39] almost completely restored CPL formation **(Fig. 4a)**, demonstrating that AGO2 promotes CPL assembly by restraining proteasome activity. To further define the temporal window during which proteasome suppression is required, we activated proteasome activity at different time points in follicle culture system and assessed CPL formation in FGO. Proteasome activation during the early window of CPL initiation (0–3 days after SF) strongly impaired CPL assembly **(Fig. 4b)**. In contrast, activating the proteasome 6–9 days after SF, when CPLs were already assembled, did not disrupt the CPL structures **(Fig. 4b)**. These findings suggest that the nascent, soluble CPL components are vulnerable to proteasomal degradation during early growth, whereas mature CPL fibers become structurally stabilized and resistant to turnover.

Since AGO2 typically functions through small RNA–guided endonucleolytic activity, we next asked whether its catalytic activity is required for CPL maintenance. We microinjected either wild-type *Ago2* mRNA or a catalytically inactive *Ago2* mutant (*Ago2-D598A*)[40] into AGO2-KO oocytes. While wild-type AGO2 efficiently rescued CPL assembly, the slicer-dead

AGO2-D598A mutant failed to restore lattice formation **(Fig. 4c, d)**. Taken together, our data demonstrate that AGO2 maintains CPL assembly in a slicer-dependent manner by suppressing proteasome activity, thereby protecting CPL components from proteasomal degradation during a critical early window of oocyte growth.

CPLs safeguard maternal proteins from ubiquitin-mediated degradation

We next asked whether the CPL defects in AGO2-KO oocytes alter the ubiquitin landscape. Surprisingly, K48-linked ubiquitination levels were reduced in AGO2-KO oocytes (**Extended data fig. 5a**), likely due to accelerated degradation of ubiquitinated substrates caused by elevated proteasome activity, as previously reported[41]. Consistent with this idea, inhibition of proteasome activity restored K48-linked ubiquitin levels in both AGO2-KO and TLE6-KO oocytes to levels higher than those in wild-type oocytes **(Fig. 5a)**. To determine whether this altered K48 ubiquitination pattern is driven by CPL-associated ubiquitination regulators, we expressed catalytically inactive mutants of FBXW24[42], UBE2D3[31], UHRF1[43], and SKP1[44], which retain substrate-binding capacity but lack ubiquitin-conjugating activity and thus act as dominant-negative inhibitors of endogenous enzymes[45] (**Extended data fig. 5b)**. Expression of these mutants significantly restored K48 ubiquitination in both AGO2-KO and TLE6-KO oocytes **(Fig. 5a; Extended data fig. 5c)**. Proteomic analysis further showed that down-regulated proteins in AGO2-KO or TLE6-KO oocytes were restored upon expression of these inactive mutants **(Fig. 5b)**. Additionally, proteins that were increased in AGO2-KO or TLE6-KO oocytes were also rescued by these mutants **(Extended data fig. 5d)**, indicating that inhibition of the CPL-associated E2/E3 activities rescues both direct and indirect downstream proteomic consequences of CPL disruption. Together, these results support a model in which CPL defects do not cause global hyper-ubiquitination, but instead drive selective, pathway-directed degradation, mirroring a consequence of unleashed E3 ligase activity against specific substrates[46].

To further test this specificity, we then overexpressed the four CPL-associated ubiquitination regulators at increasing levels (25%, 50%, and 100% of endogenous abundance).

Higher expression progressively increased the number of down-regulated proteins in a dose-dependent manner, while fewer proteins were up-regulated **(Extended data fig. 5e)**. Notably, the overlap between down-regulated proteins and those reduced in TLE6-KO oocytes increased with expression level **(Fig. 5c)**. At endogenous-equivalent expression, 179 proteins were commonly down-regulated and significantly enriched for known CPL-stored maternal factors. **(Fig. 5c, d)**. Pathway enrichment analysis showed that these proteins are involved in essential processes for oocyte and early embryonic development, including embryo development, cell cycle progression, cytoskeletal organization, and meiosis **(Fig. 5e)**. Given that substrate specificity in ubiquitination is primarily determined by E3 ubiquitin ligases[46], we next examined whether these regulators selectively target maternal proteins. Co-expression of either SKP1–FBXW24–UBE2D3 or UHRF1–UBE2D3 complexes in oocytes led to reductions in distinct sets of proteins, both of which showed substantial overlap with proteins down-regulated in TLE6-KO oocytes **(Fig. 5f, g)**. Thus, these findings indicate that CPLs primarily function as a molecular "safebox" that sequesters critical ubiquitination regulators and shields maternal proteins from ubiquitin-mediated degradation.

To assess the physiological importance of this mechanism, we asked whether restoring ubiquitin homeostasis could rescue developmental defects. We expressed catalytically inactive ubiquitination regulators in AGO2-KO or TLE6-KO oocytes and evaluated embryonic competence by *in vitro* fertilization. Remarkably, this intervention rescued the complete 1–2 cell arrest in AGO2-KO embryos to ~40% blastocyst formation and improved TLE6-KO embryos development from a 4-cell–morula arrest to ~50% blastocyst formation **(Fig. 5h, i)**.

Together, these results suggest that CPL-mediated protection of maternal protein reservoir is achieved by spatially constraining critical ubiquitination machinery. This unique mechanism enables long-term maternal proteostasis and is essential for early embryonic development.

Discussion

How oocytes sustain the maternal proteome long enough to launch embryonic development has long been unresolved. Here, we demonstrate that CPL acts as a structural safeguard by sequestering four key ubiquitination regulators—UHRF1, FBXW24, SKP1, and UBE2D3—during oocyte growth, thereby suppressing ubiquitination and preventing degradation of maternal proteins. Concurrently, an AGO2–small RNA pathway inhibits proteasome activity, reinforcing CPL integrity and maternal proteome stability. Together, CPL co-opted AGO2 to function in a ratchet-like mechanism that establishes the CPL as a protective "safebox", locking ubiquitination regulators and suppressing proteolysis to preserve the maternal proteome for faithful transmission and embryogenesis **(Fig. 6; Supplementary video 1)**. Our findings uncover a previously unrecognized strategy of proteolytic regulation that solves a long-standing puzzle: how oocytes maintain a stable maternal proteome over exceptionally long developmental timescales.

Oocyte biology is defined by the accumulation and long-lasting preservation of maternal proteins essential for embryogenesis[4,26,47]. Previous studies showed that disruption of CPL leads to early embryonic arrest and widespread loss of maternal proteins, of which many involved in essential processes such as chromosome organization, spindle dynamics, and cell-cycle regulation[21]. Based on these observations, CPLs were proposed as a storage depot for maternal factors, supplying essential proteins immediately after fertilization to initiate embryonic activation[21,26]. However, the persistence of CPLs through early embryogenesis and the absence of visible protein cargo by cryo–electron tomography[21] challenge the notion of direct physical storage. Here, we propose an alternative mechanism: rather than storing maternal proteins, CPLs function as a regulatory scaffold that sequesters key ubiquitination regulators during oogenesis. This spatial confinement limits ubiquitination and suppresses proteasomal degradation, thereby stabilizing the maternal proteome. Importantly, overexpression of these ubiquitination regulators mimics CPL disruption, driving degradation of proteins previously proposed to be stored within CPLs. Conversely, expression of ubiquitination-deficient mutants of these regulators in TLE6-KO oocytes rescues both aberrant protein loss and developmental arrest. Together, these findings support a model in which CPLs

stabilize hundreds of maternal proteins primarily by locking ubiquitination regulators and suppressing their activity, while a few proteins (SPIN1, 14-3-3 proteins, and KDM2B)[21] may be partially protected through passive storage.

Protein ubiquitination and degradation are central to proteostasis and essential for cellular health and identity across all cell types[48-50]. Ubiquitination, catalyzed by E2 and E3 enzymes, is commonly regulated through control of E3 abundance or the specificity of E2–E3–substrate interactions—a mechanism conserved across diverse processes such as spindle assembly and neural development[50-52]. However, the extended lifespan of oocytes and their need to preserve a vast maternal proteome suggest a distinct mode of ubiquitination control. Maintaining proteome stability over prolonged periods demands exceptional suppression of the ubiquitin-proteasome system. Our findings reveal a novel mechanism: during oogenesis, superstable CPLs assembling sequesters key ubiquitination regulators, thereby for a long time suppressing ubiquitination and protein degradation. Notably, these ubiquitination regulators are among the most highly expressed E2/E3 components in oocytes **(Extended data fig. 6)**. UBE2D3 and UHRF1 are the most abundant E2 and E3 enzymes, respectively, in oocytes, while SKP1 and FBXW24 are the dominant core components of the SCF ubiquitin ligase complex[53,54]. Their structural compatibility with CPL filaments further supports a dedicated sequestration mechanism via molecular fit **(Extended data fig. 7a-d)**. The high abundance of UBE2D3 and its incorporation into CPLs align with the prevalence of these structures. UBE2D3 shares high structural similarity with UBE2N that is far less abundant and might integrate into CPLs. By targeting the most influential drivers of ubiquitination, CPLs achieve efficient suppression of UPS activity. Studies have shown that CPL structures disassemble after 8-cell stage[21], coinciding with ZGA completion and the onset of large-scale maternal protein clearance[4,29], suggesting that release of sequestered ubiquitin components enables prompt turnover. Thus, the CPL might provide a temporally coordinated strategy: it suppresses UPS activity during oocyte growth to preserve the maternal proteome integrity and relinquishes this suppression after ZGA to enable maternal protein clearance. This switch from protection to turnover warrants further investigation.

Loss of AGO2 in mouse oocytes results in early embryonic arrest, a phenotype strikingly

similar to that of CPL-deficient oocytes[55,56]. Although AGO2 was previously thought to function mainly in transposon silencing in mouse oocytes, its physiological roles in embryogenesis remained unclear[57,58]. We show that enhanced proteasome activity upon AGO2 depletion destabilizes CPL components and disrupts proper CPL assembly. Moreover, CPL formation requires the slicer activity of AGO2, linking small RNA-guided endonuclease function to the architectural integrity of CPL structure **(Fig. 4c, d)**. Our previous work demonstrated that, in MII oocytes, AGO2 guided by endo-siRNAs directly cleaves multiple proteasome subunit transcripts, thereby restraining proteasome activity[59]. However, how AGO2/endo-siRNAs regulate proteasome activity during oocyte growth to support CPL assembly remains to be further elucidated. Together, we propose that like a "BoxLock", inhibition of proteasome activity by the small RNA/Argonaute pathway enables oocytes to secure the ubiquitin "safebox" of CPLs, thereby guarantying proteostasis throughout the prolonged phases of oocyte maturation and early embryogenesis **(Fig. 6)**. This rapid, coordinated system between Argonaute and CPLs offers flexible regulation and effectively shuts down the ubiquitin-proteasome system (UPS), rapidly minimizing protein perturbation.

Acknowledgements

We thank members of Shen's lab for discussions; Microscopy Imaging Core Facility of Westlake University for technical support and facility access; Mass Spectrometry & Metabolomics Core Facility of Westlake University for assistance and discussion. This work was supported by State Key Laboratory of Gene Expression (10111011A102501/003), Westlake Education Foundation, Zhejiang Provincial Foundation of China (2021R01013), the National Natural Science Foundation of China (32070628), Westlake Education Foundation (041010140118), Zhejiang Provincial Key Laboratory Construction Project, and the Westlake Laboratory of Life Sciences to E.S.

Author Contributions

Conceptualization: E.S., J.X., and S.L.; Methodology: J.X., S.L., L.X, and B.L.; Investigation: J.X., S.L., L.X., B.L., Z.L., Y.L., and E.S.; Formal analysis and Visualization: J.X., S.L., L.X, and Y.Z., Writing-Original draft: J.X., S.L., L.X., and Y.L.; Writing-Review & Editing: J.X., S.L., and E.S.; Supervision and Project administration: E.S..

Conflict of Interest

The authors declare no conflict of interest.

References

1 Zaffagnini, G. *et al.* Mouse oocytes sequester aggregated proteins in degradative super-organelles. *Cell* **187**, 1109-1126 e1121, doi:10.1016/j.cell.2024.01.031 (2024).

2 Bomba-Warczak, E. K. *et al.* Exceptional longevity of mammalian ovarian and oocyte macromolecules throughout the reproductive lifespan. *Elife* **13**, doi:10.7554/eLife.93172 (2024).

3 Harasimov, K. *et al.* The maintenance of oocytes in the mammalian ovary involves extreme protein longevity. *Nat Cell Biol* **26**, 1124-1138, doi:10.1038/s41556-024-01442-7 (2024).

4 Zhang, H. *et al.* Stable maternal proteins underlie distinct transcriptome, translatome, and proteome reprogramming during mouse oocyte-to-embryo transition. *Genome Biol* **24**, 166, doi:10.1186/s13059-023-02997-8 (2023).

5 Faddy, M. J., Gosden, R. G., Gougeon, A., Richardson, S. J. & Nelson, J. F. Accelerated disappearance of ovarian follicles in mid-life: implications for forecasting menopause. *Hum Reprod* **7**, 1342-1346, doi:10.1093/oxfordjournals.humrep.a137570 (1992).

6 Rodriguez-Nuevo, A. *et al.* Oocytes maintain ROS-free mitochondrial metabolism by suppressing complex I. *Nature* **607**, 756-761, doi:10.1038/s41586-022-04979-5 (2022).

7 Schulz, K. N. & Harrison, M. M. Mechanisms regulating zygotic genome activation. *Nat Rev Genet* **20**, 221-234, doi:10.1038/s41576-018-0087-x (2019).

8 Kojima, M. L., Hoppe, C. & Giraldez, A. J. The maternal-to-zygotic transition: reprogramming of the cytoplasm and nucleus. *Nat Rev Genet* **26**, 245-267, doi:10.1038/s41576-024-00792-0 (2025).

9 Balch, W. E., Morimoto, R. I., Dillin, A. & Kelly, J. W. Adapting proteostasis for disease intervention. *Science* **319**, 916-919, doi:10.1126/science.1141448 (2008).

10 Powers, E. T., Morimoto, R. I., Dillin, A., Kelly, J. W. & Balch, W. E. Biological and chemical approaches to diseases of proteostasis deficiency. *Annu Rev Biochem* **78**, 959-991, doi:10.1146/annurev.biochem.052308.114844 (2009).

11 Hipp, M. S., Kasturi, P. & Hartl, F. U. The proteostasis network and its decline in ageing. *Nat Rev Mol Cell Biol* **20**, 421-435, doi:10.1038/s41580-019-0101-y (2019).

12 Pohl, C. & Dikic, I. Cellular quality control by the ubiquitin-proteasome system and autophagy. *Science* **366**, 818-822, doi:10.1126/science.aax3769 (2019).

13 Ciechanover, A. Proteolysis: from the lysosome to ubiquitin and the proteasome. *Nat Rev Mol Cell Biol* **6**, 79-87, doi:10.1038/nrm1552 (2005).

14 Cruz Walma, D. A., Chen, Z., Bullock, A. N. & Yamada, K. M. Ubiquitin ligases: guardians of mammalian development. *Nat Rev Mol Cell Biol* **23**, 350-367, doi:10.1038/s41580-021-00448-5 (2022).

15 Wu, Y., Li, M. & Yang, M. Post-Translational Modifications in Oocyte Maturation and Embryo Development. *Front Cell Dev Biol* **9**, 645318, doi:10.3389/fcell.2021.645318 (2021).

16 He, M., Zhang, T., Yang, Y. & Wang, C. Mechanisms of Oocyte Maturation and Related Epigenetic Regulation. *Front Cell Dev Biol* **9**, 654028, doi:10.3389/fcell.2021.654028 (2021).

17 King, R. W., Deshaies, R. J., Peters, J. M. & Kirschner, M. W. How proteolysis drives

the cell cycle. *Science* **274**, 1652-1659, doi:10.1126/science.274.5293.1652 (1996).

18 Rousseau, A. & Bertolotti, A. Regulation of proteasome assembly and activity in health and disease. *Nat Rev Mol Cell Biol* **19**, 697-712, doi:10.1038/s41580-018-0040-z (2018).

19 Weakley, B. S. Comparison of cytoplasmic lamellae and membranous elements in the oocytes of five mammalian species. *Z Zellforsch Mikrosk Anat* **85**, 109-123, doi:10.1007/BF00330591 (1968).

20 Hadek, R. Cytoplasmic whorls in the golden hamster oocyte. *J Cell Sci* **1**, 281-282, doi:10.1242/jcs.1.3.281 (1966).

21 Jentoft, I. M. A. *et al.* Mammalian oocytes store proteins for the early embryo on cytoplasmic lattices. *Cell* **186**, 5308-5327 e5325, doi:10.1016/j.cell.2023.10.003 (2023).

22 Tashiro, F. *et al.* Maternal-effect gene Ces5/Ooep/Moep19/Floped is essential for oocyte cytoplasmic lattice formation and embryonic development at the maternal-zygotic stage transition. *Genes Cells* **15**, 813-828, doi:10.1111/j.1365-2443.2010.01420.x (2010).

23 Qin, D. *et al.* The subcortical maternal complex protein Nlrp4f is involved in cytoplasmic lattice formation and organelle distribution. *Development* **146**, doi:10.1242/dev.183616 (2019).

24 Gao, Z. *et al.* Zbed3 participates in the subcortical maternal complex and regulates the distribution of organelles. *J Mol Cell Biol* **10**, 74-88, doi:10.1093/jmcb/mjx035 (2018).

25 Liu, S. *et al.* Molecular basis of oocyte cytoplasmic lattice assembly. *Nature*, doi:10.1038/s41586-026-10360-7 (2026).

26 Yurttas, P. *et al.* Role for PADI6 and the cytoplasmic lattices in ribosomal storage in oocytes and translational control in the early mouse embryo. *Development* **135**, 2627-2636, doi:10.1242/dev.016329 (2008).

27 Morency, E., Anguish, L. & Coonrod, S. Subcellular localization of cytoplasmic lattice-associated proteins is dependent upon fixation and processing procedures. *PLoS One* **6**, e17226, doi:10.1371/journal.pone.0017226 (2011).

28 Tan, L. *et al.* Aberrant cytoplasmic expression of UHRF1 restrains the MHC-I-mediated anti-tumor immune response. *Nat Commun* **15**, 8569, doi:10.1038/s41467-024-52902-5 (2024).

29 Chen, F. *et al.* Comparative maternal protein profiling of mouse biparental and uniparental embryos. *Gigascience* **11**, doi:10.1093/gigascience/giac084 (2022).

30 Guan, Y. *et al.* SKP1 drives the prophase I to metaphase I transition during male meiosis. *Sci Adv* **6**, eaaz2129, doi:10.1126/sciadv.aaz2129 (2020).

31 Yalcin, Z. *et al.* Ubiquitinome Profiling Reveals in Vivo UBE2D3 Targets and Implicates UBE2D3 in Protein Quality Control. *Mol Cell Proteomics* **22**, 100548, doi:10.1016/j.mcpro.2023.100548 (2023).

32 Kolla, S., Ye, M., Mark, K. G. & Rape, M. Assembly and function of branched ubiquitin chains. *Trends Biochem Sci* **47**, 759-771, doi:10.1016/j.tibs.2022.04.003 (2022).

33 Cao, L., Liu, X., Zheng, B., Xing, C. & Liu, J. Role of K63-linked ubiquitination in cancer. *Cell Death Discov* **8**, 410, doi:10.1038/s41420-022-01204-0 (2022).

34 Zhou, W., Wei, W. & Sun, Y. Genetically engineered mouse models for functional

studies of SKP1-CUL1-F-box-protein (SCF) E3 ubiquitin ligases. *Cell Res* **23**, 599-619, doi:10.1038/cr.2013.44 (2013).

35 Wang, Y. *et al.* FBXW24 controls female meiotic prophase progression by regulating SYCP3 ubiquitination. *Clin Transl Med* **12**, e891, doi:10.1002/ctm2.891 (2022).

36 Okamoto, S. Y., Sato, M., Toda, T. & Yamamoto, M. SCF ensures meiotic chromosome segregation through a resolution of meiotic recombination intermediates. *PLoS One* **7**, e30622, doi:10.1371/journal.pone.0030622 (2012).

37 Zhang, H. *et al.* H3K27me3 shapes DNA methylome by inhibiting UHRF1-mediated H3 ubiquitination. *Sci China Life Sci* **65**, 1685-1700, doi:10.1007/s11427-022-2155-0 (2022).

38 Zaffagnini, G., Sole, M., Duran, J. M., Polyzos, N. P. & Boke, E. The proteostatic landscape of healthy human oocytes. *EMBO J* **44**, 4611-4630, doi:10.1038/s44318-025-00493-2 (2025).

39 Kisselev, A. F. Site-Specific Proteasome Inhibitors. *Biomolecules* **12**, doi:10.3390/biom12010054 (2021).

40 Cheloufi, S., Dos Santos, C. O., Chong, M. M. & Hannon, G. J. A dicer-independent miRNA biogenesis pathway that requires Ago catalysis. *Nature* **465**, 584-589, doi:10.1038/nature09092 (2010).

41 Vilchez, D. *et al.* Increased proteasome activity in human embryonic stem cells is regulated by PSMD11. *Nature* **489**, 304-308, doi:10.1038/nature11468 (2012).

42 Schulman, B. A. *et al.* Insights into SCF ubiquitin ligases from the structure of the Skp1-Skp2 complex. *Nature* **408**, 381-386, doi:10.1038/35042620 (2000).

43 Foster, B. M. *et al.* Critical Role of the UBL Domain in Stimulating the E3 Ubiquitin Ligase Activity of UHRF1 toward Chromatin. *Mol Cell* **72**, 739-752 e739, doi:10.1016/j.molcel.2018.09.028 (2018).

44 Zheng, N. *et al.* Structure of the Cul1-Rbx1-Skp1-F boxSkp2 SCF ubiquitin ligase complex. *Nature* **416**, 703-709, doi:10.1038/416703a (2002).

45 von der Lehr, N. *et al.* The F-box protein Skp2 participates in c-Myc proteosomal degradation and acts as a cofactor for c-Myc-regulated transcription. *Mol Cell* **11**, 1189-1200, doi:10.1016/s1097-2765(03)00193-x (2003).

46 Timms, R. T. *et al.* Defining E3 ligase-substrate relationships through multiplex CRISPR screening. *Nat Cell Biol* **25**, 1535-1545, doi:10.1038/s41556-023-01229-2 (2023).

47 Fuentes, R. *et al.* Maternal regulation of the vertebrate oocyte-to-embryo transition. *PLoS Genet* **20**, e1011343, doi:10.1371/journal.pgen.1011343 (2024).

48 Zhao, L., Zhao, J., Zhong, K., Tong, A. & Jia, D. Targeted protein degradation: mechanisms, strategies and application. *Signal Transduct Target Ther* **7**, 113, doi:10.1038/s41392-022-00966-4 (2022).

49 Wolff, S., Weissman, J. S. & Dillin, A. Differential scales of protein quality control. *Cell* **157**, 52-64, doi:10.1016/j.cell.2014.03.007 (2014).

50 Gao, M. & Karin, M. Regulating the regulators: control of protein ubiquitination and ubiquitin-like modifications by extracellular stimuli. *Mol Cell* **19**, 581-593, doi:10.1016/j.molcel.2005.08.017 (2005).

51 Hale, M. & Bashaw, G. J. Emerging roles for E3 ubiquitin ligases in neural development

and disease. *Front Cell Dev Biol* **13**, 1557653, doi:10.3389/fcell.2025.1557653 (2025).

52 Bellaart, A. *et al.* TRIM37 prevents ectopic spindle pole assembly by peptide motif recognition and substrate-dependent oligomerization. *Nat Struct Mol Biol* **32**, 1800-1811, doi:10.1038/s41594-025-01562-0 (2025).

53 Jia, L. & Sun, Y. SCF E3 ubiquitin ligases as anticancer targets. *Curr Cancer Drug Targets* **11**, 347-356, doi:10.2174/156800911794519734 (2011).

54 Skaar, J. R., Pagan, J. K. & Pagano, M. Mechanisms and function of substrate recruitment by F-box proteins. *Nat Rev Mol Cell Biol* **14**, 369-381, doi:10.1038/nrm3582 (2013).

55 Zhang, J. M. *et al.* Argonaute 2 is a key regulator of maternal mRNA degradation in mouse early embryos. *Cell Death Discov* **6**, 133, doi:10.1038/s41420-020-00368-x (2020).

56 Giaccari, C., Cecere, F., Argenziano, L., Pagano, A. & Riccio, A. New insights into oocyte cytoplasmic lattice-associated proteins. *Trends Genet* **40**, 880-890, doi:10.1016/j.tig.2024.06.002 (2024).

57 Stein, P. *et al.* Essential Role for endogenous siRNAs during meiosis in mouse oocytes. *PLoS Genet* **11**, e1005013, doi:10.1371/journal.pgen.1005013 (2015).

58 Watanabe, T. *et al.* Endogenous siRNAs from naturally formed dsRNAs regulate transcripts in mouse oocytes. *Nature* **453**, 539-543, doi:10.1038/nature06908 (2008).

59 Xue, J. *et al.* A novel proteasome-ribosome axis regulated by endogenous siRNAs in oocytes governs maternal-to-zygotic transition. *Vita*, (2026).

60 So, C. *et al.* Mechanism of spindle pole organization and instability in human oocytes. *Science* **375**, eabj3944, doi:10.1126/science.abj3944 (2022).

61 Li, Z. *et al.* Mammalian PIWI-piRNA-target complexes reveal features for broad and efficient target silencing. *Nat Struct Mol Biol* **31**, 1222-1231, doi:10.1038/s41594-024-01287-6 (2024).

62 Li, Z. *et al.* Structural insights into RNA cleavage by PIWI Argonaute. *Nature* **639**, 250-259, doi:10.1038/s41586-024-08438-1 (2025).

63 Huypens, P. *et al.* Epigenetic germline inheritance of diet-induced obesity and insulin resistance. *Nat Genet* **48**, 497-499, doi:10.1038/ng.3527 (2016).

Methods

Mice

Wild type female C57BL/6J mice, *Ago2*$^{loxP/loxP,\ Zp3\text{-}cre}$ female mice were maintained in specific pathogen-free environment animal facility of Westlake University with strictly controlled macroenvironment, including a temperature of 20-26℃, humidity ranges of 40-70%, and a 12-hour light/12-hour dark cycle. All animal experiments and protocols were conducted in compliance with institutional guidelines, our animal care and use protocol (AP#25-065-SEZ) was approved by the Institutional Animal Care and Use Committee of Westlake University, Hangzhou, China.

Tle6-knockout mice were a kind gift from Dr. Dong Deng (State Key Laboratory of Biotherapy, Sichuan University). Mice were backcrossed into the C57BL/6J background. For amplifying the wild-type *Tle6* allele, the following primers were used: 5'-TCAGGGCTTGGGTATTGTCCA-3' and 5'-GTGCCCCCTGCACATAAGTA-3', which amplify a 422-bp fragment. For amplifying the knockout *Tle6* allele, the following primers were used: 5'-CTGATCCCGCTAGGGAGTTG-3' and 5'-GTGCCCCCTGCACATAAGTA-3', which yield a 335-bp product specific to the knockout allele.

Cell line

HEK-293F cells were cultured in SMM 293-II medium (Sino Biological), supplemented with 1% (v/v) penicillin–streptomycin (Gibco), at 37℃ under 5% CO_2 for plasmid transfection and recombinant protein expression and purification. Sf9 cells for plasmid transfection and protein purification were cultured in SF900 II SFM medium (Sino Biological), supplemented with 1% penicillin-streptomycin (Gibco) at 27℃.

Bacterial strains

Molecular cloning was performed in DH5α Chemically Competent *Escherichia coli* (*E. coli*) (Vazyme). Recombinant proteins were expressed in transformed *E. coli* BL21 ER2566 competent cells (Tsingke) cultured in LB medium as appropriate. Cells were grown in LB supplemented with appropriate antibiotics at 37℃.

Preparation and culture of mouse oocytes

Secondary follicles were isolated from 10-12-day-old female mice following a previously described procedure[60], and all granulosa cells were subsequently removed. 14-day-old female mice were sacrificed to collect growing oocytes. 4-week-old female mice were super-ovulated by intraperitoneal injection with 10 U pregnant mare serum gonadotropin (PMSG) (Aibei). Fully grown oocytes (~75 μm) were harvest for experiments and cultured in M2 medium (Aibei) supplied with 2.5 μM milrinone (Sigma-Aldric) covered with mineral oil (Fisher Chemical™) at 37℃. To obtain in vitro maturation oocytes, GVBD oocytes and MI oocytes were harvested and fixed at different timepoints after with 2.5 μM milrinone (Sigma-Aldric) release. For MII oocytes, 10U human chorionic gonadotropin (hCG) (Aibei) were injected into the mice that had previously been primed with PMSG 48 hours earlier. Cumulus-oocyte complexes were collected and fixed 13-14 h after hCG injection.

Transmission electron microscopy (TEM) imaging

Wild-type oocytes at different developmental stages and AGO2-KO oocytes were manually dissected and fixed overnight at 4°C in 2% glutaraldehyde prepared in 0.1 M sodium cacodylate buffer (pH 7.4). Following fixation, oocytes were embedded in 2% agarose. Agarose blocks containing individual oocytes were excised and washed three times with ice-cold 0.1 M sodium cacodylate buffer. Following fixation, agarose blocks were post-fixed in 1% reduced osmium tetroxide in cacodylate buffer for 1 h, washed three times with 0.1 M sodium cacodylate buffer and ddH_2O, and stained with 1% uranyl acetate in ddH_2O for 1 h. After dehydration in a graded ethanol series, blocks were infiltrated with Durcupan ACM resin. Ultrathin sections were cut and imaged using a Talos L120C G2 TEM (Thermo Scientific) at 80 kV.

RT-qPCR

40 mouse oocytes (per sample) were extensively washed in phosphate-buffered saline (PBS). Total RNA was extracted with TRIzol LS Reagent (Thermo Fisher Scientific). Reverse transcription (RT) was performed using NovoScript One-Step RT-PCR Kit (Novoprotein), and quantitative PCR (qPCR) was performed using ChamQ Universal SYBR qPCR Master Mix (Vazyme) on a LightCycler® 96 Instrument (Roche). Endogenous *Gapdh* was used as an

internal control to calculate relative transcript level. Primers used in the study are described in supplementary Table 1.

Immunoprecipitation, pulldown, and immunoblotting

Oocytes were lysed in NP-40 lysis buffer (Solarbio) containing 1× cOmplete™ EDTA-free protease inhibitor cocktail (Roche). Lysates were incubated on ice for 10 min and centrifuged at 12,000 × g for 10 min at 4℃. Supernatants were incubated with TUBE 2 (Magnetic Beads) for 2 h at 4℃, followed by washing five times with PBS, and bound proteins were eluted, resolved by SDS–PAGE, and analyzed by immunoblotting using the indicated antibodies.

PADI6 WT or mutant proteins mixed with FBXW24 and SKP1 proteins or UHRF1 and UBE2D3 proteins were incubated with DYKDDDDK nanoab magnetic beads (LABLEAD) for 1 h at 4℃. The beads were washed three times with buffer (25 mM Tris-HCl, pH 8.0, 150 mM NaCl, 0.1% Triton X-100). Proteins bound to the DYKDDDDK nanoab magnetic beads were eluted with 0.4 mg/mL FLAG peptide. Input and immunoprecipitated fractions were resolved by SDS-PAGE and analyzed by immunoblotting using the indicated antibodies.

For immunoblots, oocytes at different stages from wildtype mice, FGO oocytes from wildtype and AGO2-KO mice were loaded into each lane. The collected cells were lysed by incubating them on ice for 10 minutes in lysis buffer (50 mM Tris, pH 7.6, 150 mM NaCl, 1% Igepal CA-630, 0.5% sodium deoxycholate, 0.1% SDS) supplemented with 1× cOmplete™ EDTA-free protease inhibitor cocktail (Roche). The lysed cells were then centrifuged at >16,000 g for 10 minutes at 4℃, and the supernatant was boiled at 95℃ for 5 minutes. Samples were resolved on 4-12% PAGE gels (Genscript) and run at 130V for ~1 h in MOPS buffer (25 mM Tris and 192 mM glycine). Proteins were transferred onto 0.45 mm PVDF membranes for 15 min with an eBlot L1 Fast Wet Transfer System (Genscript), PVDF membranes were blocked with 5% milk TBS with 0.1% Tween-20 (TBST) for 1 h at room temperature, and then incubated with primary antibody overnight at 4℃ followed by horseradish peroxidase (HRP)-conjugated secondary antibody incubation for 1 h at room temperature, with 4 washes of PBS with 0.1% Tween-20 (PBST) before imaging with ChemiDoc Imagers (Bio-rad). Antibodies used include anti-NLRP14 (Abnova), anti-UHRF1 (ABclonal), anti-UBE2D3 (Novus), anti-FBXW24 (Hangzhou leqi), anti-SKP1 (Selleck), anti-

TUBB2A/B (Sigma-Aldrich), anti-MATER (Abcam), anti-NLRP4f (Bioss), anti-FLOPED (Biosynth), anti-FILIA (Hangzhou leqi), anti-PADI6 (Thermo Fisher Scientific), anti-TLE6 (Thermo Fisher Scientific), anti-GAPDH (Abcam), anti-K48 (Abcam), anti-K63 (Biodragon), Goat anti-Rabbit IgG (H+L) HRP (Jackson Immunoresearch), and Goat anti-Mouse IgG (H+L) HRP (Jackson Immunoresearch). Chemiluminescence was performed with enhanced chemiluminescence (ECL) reagent (Biosharp) and imaged with ChemiDoc Imagers (Bio-rad).

CPL extraction

Oocytes were isolated and immediately lysed in 10 μL of a buffer containing 10 mM HEPES (pH 7.3), 0.2 M sucrose, 50 mM KCl, 0.5% Triton X-100, and 1 mM PMSF using a pulled Pasteur pipette with ~60 μm inner diameter[26]. For input control, an aliquot of whole-cell lysate was reserved prior to centrifugation. The remaining lysate was centrifuged at 650 × g for 5 min. The supernatant was transferred and further centrifuged at 9,000 × g for 5 min. For immunoblotting, an aliquot of the resulting 9,000 × g supernatant was mixed with 5 × SDS sample buffer (250 mM Tris·HCl, pH 6.8, 10% SDS, 30% Glycerol, 10 mM DTT, 0.05% bromophenol blue) and analyzed by SDS–PAGE. The pellet was washed three times with 1 mL PBS, resuspended in 5 × SDS sample buffer, and subjected to immunoblotting.

Immunofluorescence staining

Oocytes were fixed for 30 min at 37℃ in a buffer containing 100 mM HEPES (pH 7.0, titrated with KOH), 50 mM EGTA (pH 7.0, titrated with KOH), 10 mM $MgSO_4$, 2% methanol-free formaldehyde, and 0.2% Triton X-100. After fixation, oocytes were permeabilized in PBS containing 0.5% Triton X-100 (PBT) for 30 min at room temperature, and blocked in PBT with 3% BSA (PBT-BSA) for 1 h at room temperature. Primary antibodies were applied and incubated overnight at 4℃, followed by three 15 min washes with PBT-BSA. Secondary antibodies (diluted to 5 μg/mL) were incubated for 1 h at room temperature. Primary antibodies used were rabbit anti-K48 (Abcam) and rabbit anti-K63 (Biodragon). AlexaFluor488- and 594-conjugated rabbit IgG highly cross-adsorbed secondary antibodies were used (Thermo Fisher Scientific).

Expansion microscopy

The expansion microscopy (ExM) kit is a gift from Dr. Kiryl D. Piatkevic of Westlake university. Chemically fixed oocytes were incubated with an Atto 488-NHS-ester (Sigma-Aldrich) at 10 μg/ml in PBSTT (phosphate-buffered saline with 0.1% Tween 20, 0.01% Triton-100) for 1 hour at room temperature and subsequently washed 2 × 15 minutes in 1 × PBSTT, followed by incubation in Reagent X for 30 minutes at 37℃ and subsequently washing with PBS for 3 × 5 minutes. Cells were then transferred to 20 mm glass bottom cell culture dish (Nest) and excess PBS was aspirated, leaving a layer of liquid to cover the oocytes to prevent them from drying out. Stock 8× was carefully added to cover the oocytes and then a cover slide was used to cover the dish. 200 μL activated gelation solution (95% Stock 8×, 0.3% Ammonium persulfate (APS; Thermo Fisher Scientific), 0.2% Tetramethylethylenediamine (TEMED; Thermo Fisher Scientific) was added into space between cover slide and chamber containing cells. Dish with cells was transferred for incubation for 20 minutes at 4℃ followed by an oxygen-free environment incubation for 3.5 hours at 37℃. Following gelation, the cover glass was removed by a wide-headed tweezer and carefully peeled off the fully polymerized gel. Gels were fully immersed with the digestion solution (50 mM boric acid, 0.2 M SDS, 0.1 M Tris PH 6.8, 25 mM EDTA) and incubated at 95℃ for 30 minutes for gel denaturation. Finally, gels were washed in PBS and subsequently expanded in H_2O overnight at room temperature.

In vitro mRNA synthesis and microinjection of mRNAs

Genes encoding *Uhrf1* (UniProt ID: Q8VDF2), *Fbxw24* (UniProt ID: E9PXM9), *Skp1* (UniProt ID: Q9WTX5), *Ube2d3* (UniProt ID: P61079), *Ago2* (UniProt ID: Q8CJG0) were amplified from reverse-transcribed mouse ovarian cDNA and cloned into the pGEMHE-mScarlet vector (a gift from Dr. Chun So of NIBS). *Ago2 D598A* mutant was generated using Q5 Site-Directed Mutagenesis Kit (New England Biolabs), and all constructs were verified by Sanger DNA sequencing. *Fbxw24-Δ1-25*, *Skp1-Δ95-110, Ube2d3-C85A* and *Uhrf1-Δ1-78* mutants were constructed using site-directed mutagenesis (New England Biolabs) or Gibson assembly (Vazyme). From these constructs, mRNAs were in vitro synthesized using the HiScribe T7 ARCA mRNA Kit (NEB) following the manufacturer's instructions. Mouse

oocytes were microinjected with 3.5 to 14 pl of mRNAs with Embryo microinjection system (Eppendorf). Oocytes were allowed to express the mRNAs for 3 to 4 h.

Protein expression and purification

The full-length mouse *Ube2d3* and *Uhrf1* coding sequences were expressed respectively in *E. coli* and cloned into pET28a (+) in frame with the 6 × HIS sequence. Expression vectors were transformed into BL21-ER2566 competent cells (Tsingke). The full-length mouse PADI6 and SKP1 coding sequences were expressed in HEK 293F cells (Invitrogen) and cloned into the pcDNA3.1(+) vector with an N terminal 3 × FLAG tag followed by a TEV cleavage site. The plasmid was infected transiently to HEK 293F cells. PADI6 mutants including PADI6 $^{N158A, Q162A, R173}$ and PADI6 $^{K333A, E336A, Q341A, Y380A, N586A, D653A, N658A, D661A}$ were constructed using site-directed mutagenesis (New England Biolabs) or Gibson assembly (Vazyme). The gene coding for full-length FBXW24 was cloned into pFastBac^{TM} 1 with a C-terminal FLAG tag followed by a TEV cleavage site for expression using the bac-to-bac (Invitrogen) baculovirus expression system and overexpressed in Sf9 cells. Recombinant UBE2D3 and UHRF1 proteins expressed in *E. coli* were purified as previously described[61]. SKP1, PADI6, and its mutant variants expressed in HEK-293F cells were purified according to a previously established protocol[61]. FBXW24 protein expressed in SF9 cells was purified as described previously[62].

Ubiquitin assay

Ubiquitination reactions were performed using a Ubiquitin Conjugation Assay Kit (Abcam) containing recombinant E1, ubiquitin, and conjugation initiation reagents. The reaction mixture (50 µL) included kit-supplied E1 enzyme, ubiquitin, Mg^{2+}, ATP, and reaction buffer, supplemented with 10 µg of each purified protein: Flag–SKP1, FBXW24–Flag, Flag–PADI6 (wild-type or Mutant1/2), His–MBP–UHRF1, and His–UBE2D3 (prepared in this study). CUL5, histone H3, and RAD51 were purchased from MedChemExpress (MCE). Reactions were incubated at 37°C for 4 h according to the manufacturer's instructions, terminated by addition of non-reducing buffer, and analyzed by 12% SDS–PAGE followed by immunoblotting with anti-H3 (Abcam) and anti-RAD51 (MCE) antibodies.

HEK 293F cells were co-transfected with plasmids encoding SKP1, FBXW24, and either wild-type PADI6 (PADI6-WT) or its mutant variants, or alternatively with UHRF1, UBE2D3, and PADI6-WT/Mutant, using polyethylenimine (PEI) for transient expression. The proteasome inhibitor MG132 (Selleck) was added to the culture medium. After 60 h incubation, cells were collected and proteins were extracted, and equal amounts of cell lysates were immunoblotted with an anti-K48 antibody (Abcam).

Drug treatments

Fully grown GV oocytes of wildtype and AGO2-KO mice were cultured in M2 medium. MG132 (Selleck) or Bortizomib (Selleck) was reconstituted in DMSO (Sigma-Aldrich), diluted to a final concentration of 0.05 μM or 0,025 μM in M2 buffer followed by adding to the oocytes 6 h after milrinone release. The oocytes were subsequently incubated at 37°C in a 5% CO_2 environment until the performance of expansion microscopy or IVF. HEK293 cells transfected with plasmids encoding NLRP4f^{WT}, NLRP4f^{K173R}, NLRP14^{WT}, NLRP14^{K35R}, Tle6^{WT}, Tle6^{K126R} were co-treated with cycloheximide (CHX, 10 μM) and either DMSO or MG132 and harvested at 0, 2, 4, and 8 hours after CHX treatment for immunoblot analysis. Secondary follicles were in vitro cultured and treated with a PA28γ activator (Enzo Life Sciences) at a final concentration of 2.5 μM on days 0, 3, 6, and 9, followed by maturation to the fully grown oocyte (FGO) stage and labeling with NHS-Atto488.

IVF

Oocyte isolation and IVF were conducted following standardized procedures as previously described[63]. Briefly, epididymal spermatozoa were obtained from the cauda epididymis of 8 to 10-week-old C57BL6 mice and subsequently incubated in HTF medium (Aibei) for 1 h at 37°C in an environment containing 5% CO_2, female mice were euthanized the same day at 4 weeks of age, after superovulation induced with 5 U of PMSG and 5 U of HCG before being killed for oocyte collection. The sperm and the oocytes were co-cultured for 4–6 h. Subsequently, the fertilized oocytes were transferred and incubated in KSOM medium at 37°C and 5% CO_2. Rates of different development stages were microscopically checked and measured to assess embryonic development.

MS analysis

Samples were lysed using RIPA lysis buffer followed by sonication. Total protein was reduced with 10 mM dithiothreitol at 55℃ for 45 minutes, followed by alkylation with 50 mM iodoacetamide at room temperature in the dark for 30 minutes. Purification was performed employing SP3 technology as described by Hughes et al.[63]. The purified proteins were digested with trypsin (Promega) using a 1:100 enzyme-to-protein ratio (w/w) at 37℃ overnight. The resulting peptides were then lyophilized in preparation for LC-MS/MS analysis. For LC-MS/MS, lyophilized peptides were resuspended in 20 µL of 0.1% formic acid and 3 µL aliquots were injected using the nanoElute UHPLC System (Bruker) onto a home-made 25 cm × 75 µm ID, 1.9 µm C18 column. Peptides were eluted with a gradient of water/0.1% formic acid (A) and acetonitrile/0.1% formic acid (B) over 30 minutes at a flow rate of 300 nL/min, with the linear gradients starting from 4% B and increasing to 24% in 24 min, followed by an increase to 37% B in 26 min, 80% B in 28 min, 80% B in 28–30 min. Eluted peptides were analyzed with a TIMS quadrupole time-of-flight timsTOF HT instrument (Bruker Daltonics) using a CaptiveSpray nano-electrospray source. The dda-PASEF mode was employed with a m/z range of 300 to 1500 and a 1/K0 range of 0.75-1.3, with a Ramp Time of 150 ms. LC-MS/MS data files were processed using Proteome Discoverer (version 2.5) to identify proteins using the Sequest HT search engine against the Mus musculus proteome from Uniprot (https://www.uniprot.org/). Search parameters included a peptide mass tolerance of 10 ppm for 1 isotopic peak, precursor mass range of 600-6,000 Da, and tryptic digestion specificity. Variable modifications included oxidation of methionine and carbamidomethylation of cysteine. The False Discovery Rate (FDR) was set to 1% for both protein and peptide levels. Differentially expressed proteins identified by proteomics are summarized in supplementary Table 2.

Data and materials availability

All data needed to evaluate the conclusions in the paper are present in the paper and/or the Supplementary Materials. Additional data and materials in this study are available upon request.

References

25 Yurttas, P. et al. Role for PADI6 and the cytoplasmic lattices in ribosomal storage in oocytes and translational control in the early mouse embryo. Development 135, 2627-2636, doi:10.1242/dev.016329 (2008).

60 So, C. *et al.* Mechanism of spindle pole organization and instability in human oocytes. *Science* **375**, eabj3944, doi:10.1126/science.abj3944 (2022).

61 Li, Z. *et al.* Mammalian PIWI-piRNA-target complexes reveal features for broad and efficient target silencing. *Nat Struct Mol Biol* **31**, 1222-1231, doi:10.1038/s41594-024-01287-6 (2024).

62 Li, Z. *et al.* Structural insights into RNA cleavage by PIWI Argonaute. *Nature* **639**, 250-259, doi:10.1038/s41586-024-08438-1 (2025).

63 Huypens, P. *et al.* Epigenetic germline inheritance of diet-induced obesity and insulin resistance. *Nat Genet* **48**, 497-499, doi:10.1038/ng.3527 (2016).

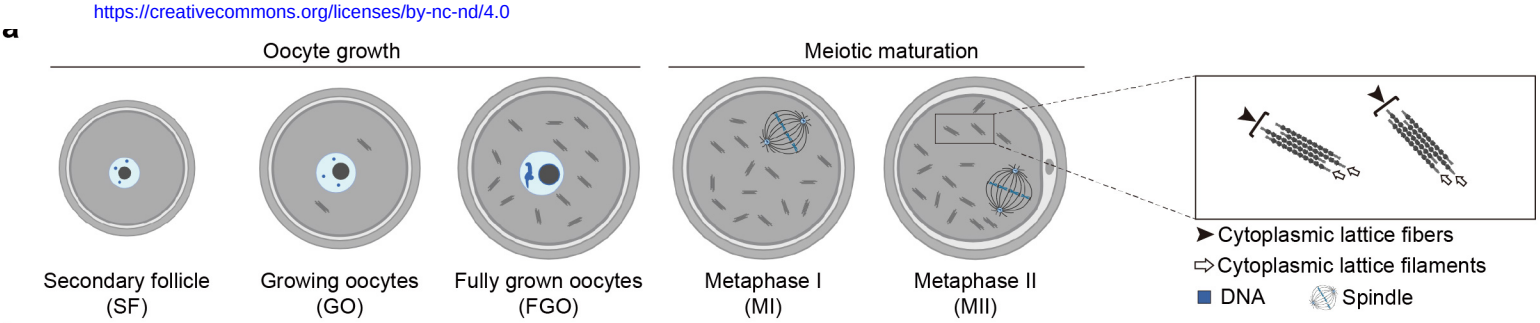

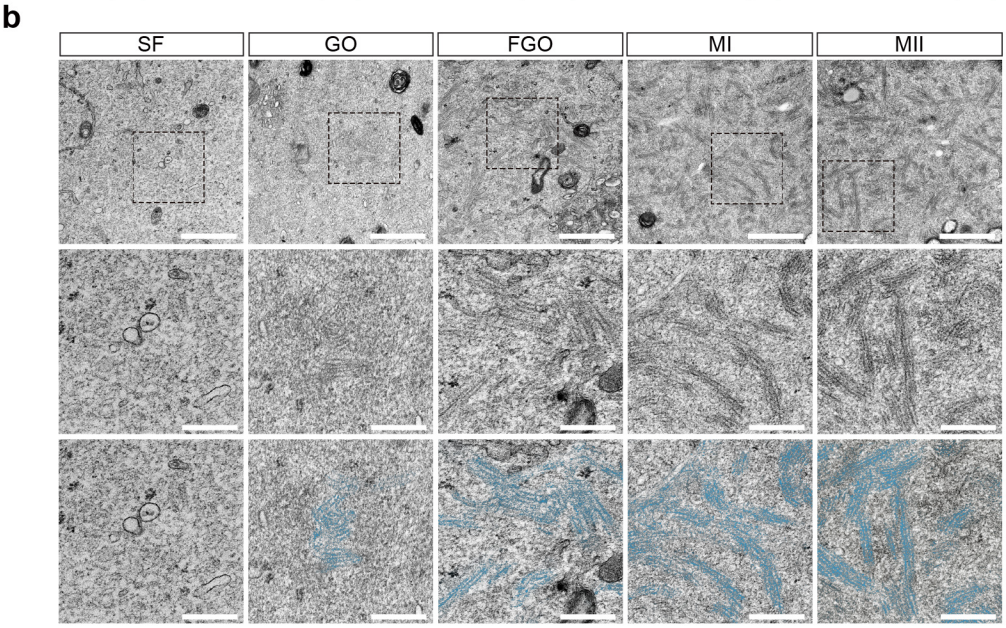

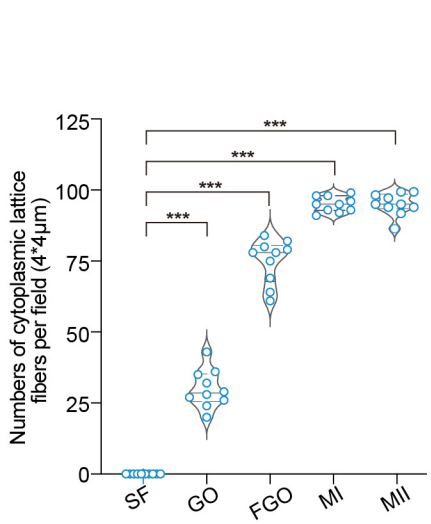

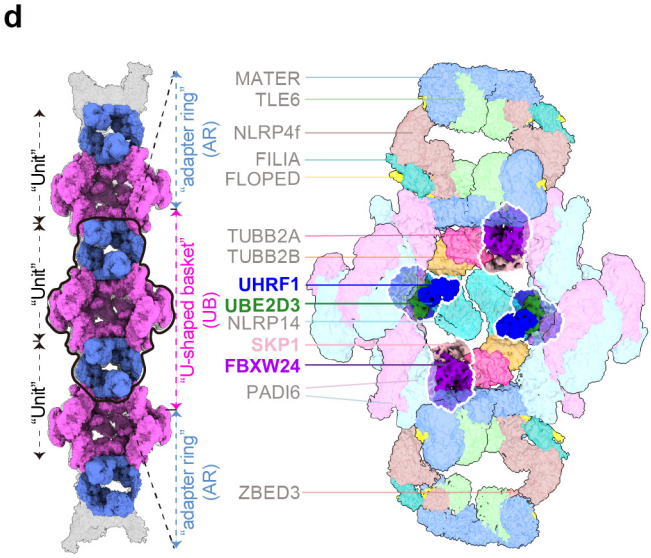

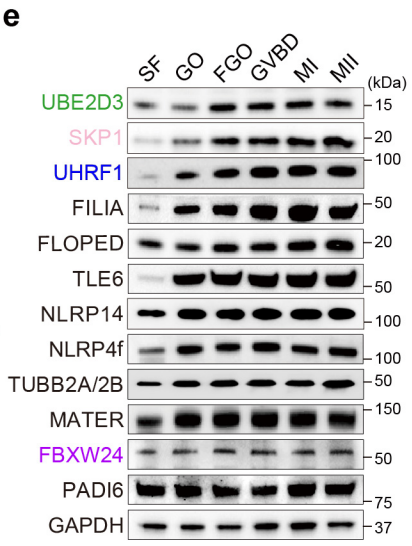

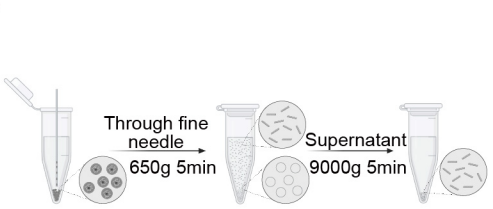

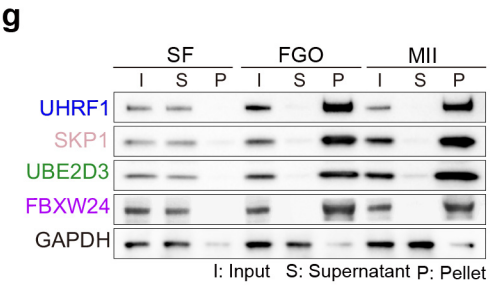

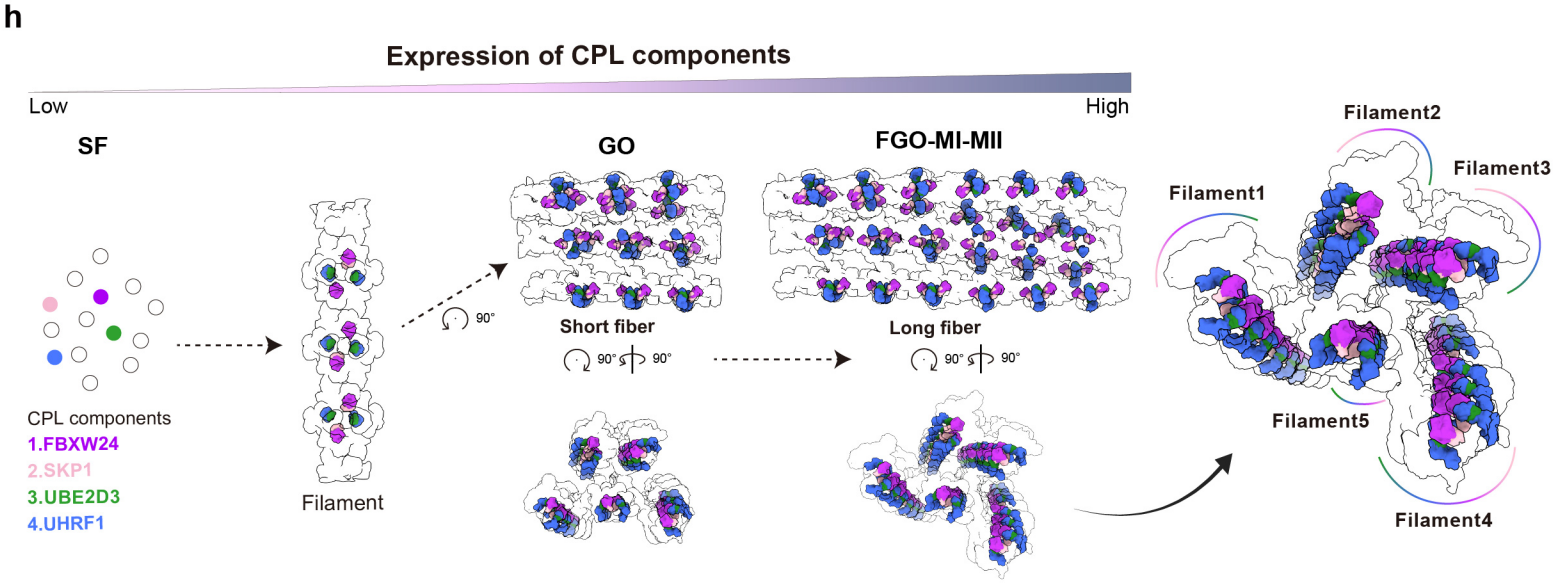

Assembly of CPL and Sequestration of Ubiquitination Regulators

Fig. 1 CPL formation sequesters ubiquitination regulators in oocytes.

a, Schematic representation of CPL dynamics during oocyte growth and meiotic maturation. **b, c**, Representative TEM images (b) and quantification (c) of CPL in different stages of oocytes. All insets are magnifications of outlined regions. Scale bar, 1 μm, scale bar of insets, 400 nm. ***$P < 0.001$, determined by unpaired two-tailed Student's *t*-test. **d**, Cryo-EM reconstruction of one UB and two ARs of the CPL, with 14 constitutive protein subunits identified and labeled. **e,** Representative immunoblots showing expression of CPL subunits during oocyte development, with GAPDH as loading control. **f,** Schematic diagram of the workflow for CPL fractionation. **g,** Representative immunoblots from CPL fractionation showing distribution of UBE2D3, SKP1, UHRF1, and FBXW24 in soluble and pellet fractions during oocyte development. **h,** Model for assembly of CPL and sequestration of ubiquitination regulators.

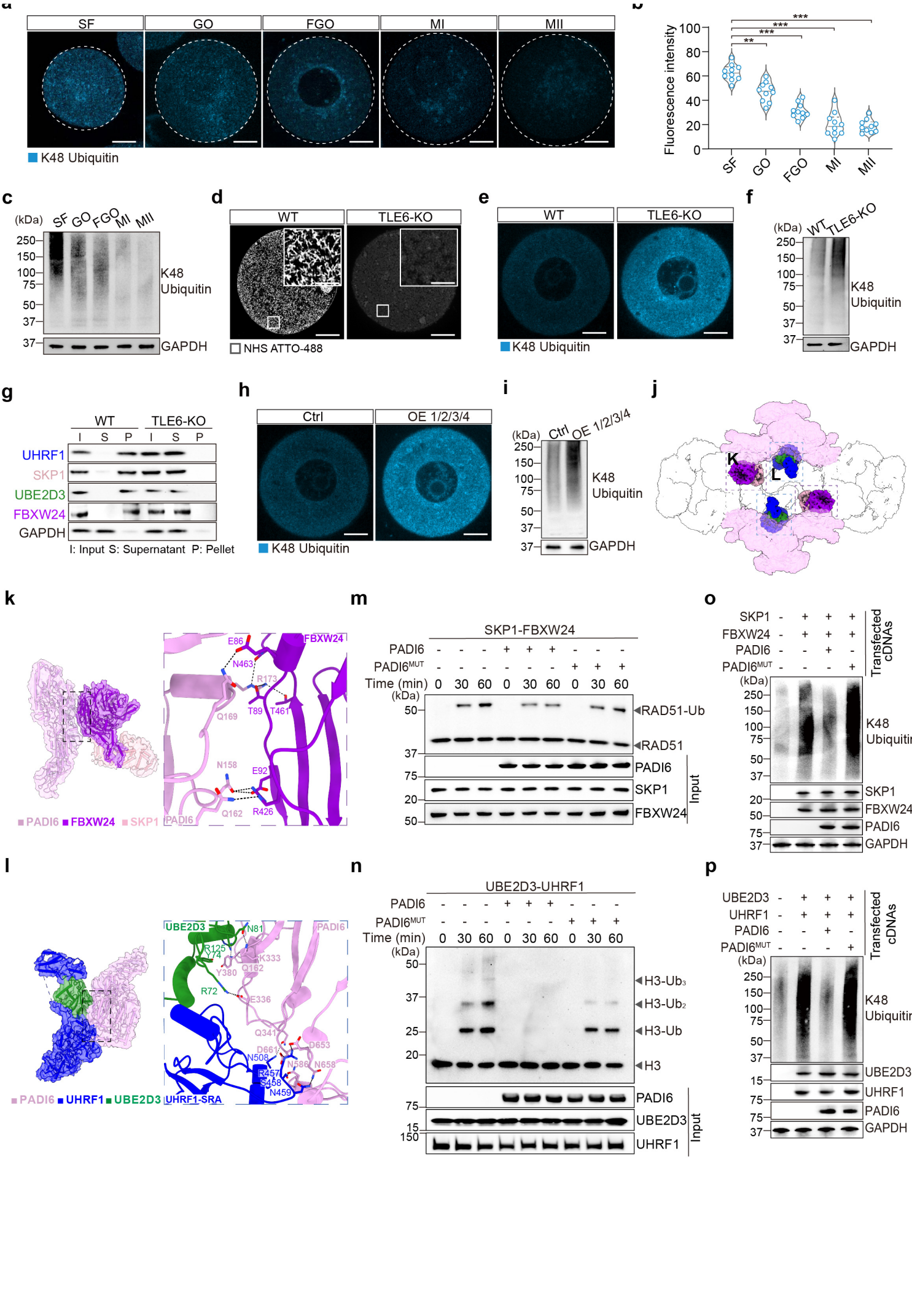

Fig. 2 CPL assembly restricts K48-linked ubiquitination in oocytes.

a, **b,** Representative micrographs (a) and quantification (b) of different stages of mouse wild-type oocytes stained with an anti-K48-linked ubiquitin antibody followed by a secondary antibody. Scale bar, 15 μm. ***$P < 0.001$, determined by unpaired two-tailed Student's *t*-test. **c**, Representative immunoblots of lysates from wild-type mouse oocytes at different developmental stages, probed with an anti-K48-linked ubiquitin antibody. **d**, Representative pan-expansion microscopy (pan-ExM) images of wild-type and TLE6-KO mouse oocytes labeled with NHS-Atto48. Scale bars, 12.5 μm, scale bar of insets, 2.5 μm. All pan-ExM micrograph scale bars are corrected for expansion factor. **e,** Representative micrographs of wild-type and TLE6-KO mouse oocytes stained with an anti-K48-linked ubiquitin antibody. Scale bar, 15 μm. **f,** Representative immunoblots of lysates from wild-type and TLE6-KO mouse oocytes detected with an anti-K48-linked ubiquitin antibody. **g,** Representative immunoblots from CPL fractionation showing distribution of UBE2D3, SKP1, and UHRF1 in soluble and pellet fractions of wild-type and TLE6-KO mouse oocytes. **h,** Representative micrographs of wild-type mouse oocytes microinjected with a mixture of *Fbxw24*, *Skp1*, *Ube2d3*, and *Uhrf1* mRNAs (OE1/2/3/4) and stained with an anti-K48-linked ubiquitin antibody. Non-injected wild-type oocytes served as controls. Scale bar, 15 μm. **i,** Representative immunoblots of lysates from wild-type oocytes and oocytes microinjected with *Fbxw24*, *Skp1*, *Ube2d3*, and *Uhrf1* mRNAs (OE1/2/3/4), probed with an anti-K48-linked ubiquitin antibody. **j,** Cryo-EM density maps of PADI6, FBXW24, SKP1, UBE2D3, and UHRF1 in UB, outlined with distinct color codes. **k,** Interactions between PADI6 and FBXW24. **l,** Interactions between PADI6, UBE2D3, and UHRF1. **m,** In vitro ubiquitination assay showing the effect of PADI6 wild-type and PADI6 mutant proteins PADI6$^{N158A, Q162A, R173A}$ on SCF (CUL1–SKP1–FBXW24)-mediated ubiquitination of the substrate RAD51. **n,** In vitro ubiquitination assay showing the effect of PADI6 wild-type and PAID6 mutant proteins PADI6$^{K333A, E336A, Q341A, Y380A, N586A, D653A, N658A, D661A}$ on UBE2D3-UHRF1-mediated ubiquitination of the substrate H3. **o,** Immunoblot analysis showing that PADI6 wild-type, but not PADI6 mutant PADI6$^{N158A, Q162A, R173A}$, suppresses SKP1–FBXW24-induced K48-linked ubiquitination in HEK293F cells. **p,** Immunoblot analysis showing that PADI6 wild-type, but not mutant PADI6

790 K333A, E336A, Q341A, Y380A, N586A, D653A, N658A, D661A, suppresses UBE2D3-UHRF1-induced K48-

791 linked ubiquitination in HEK293F cells.

792

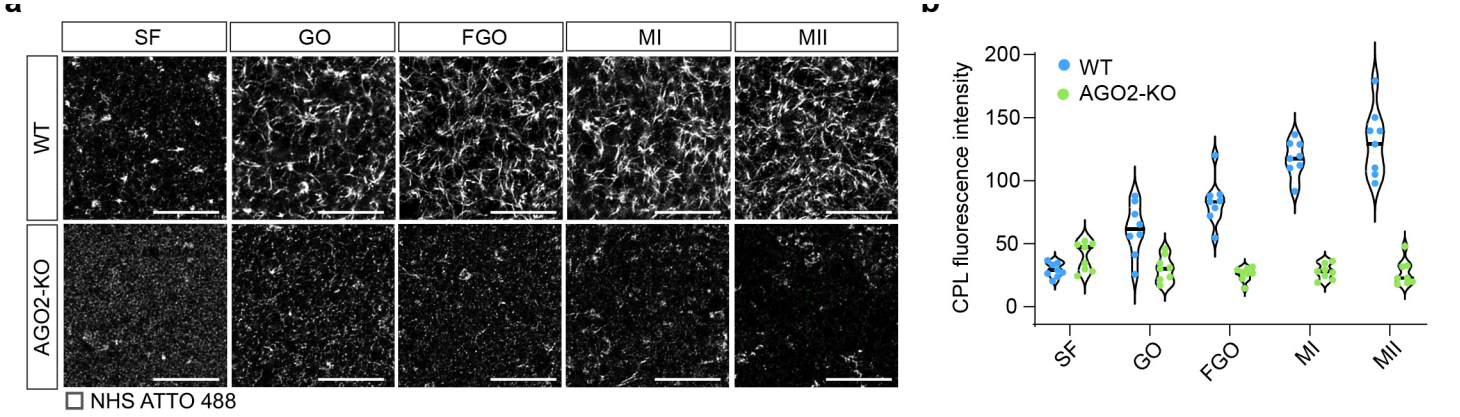

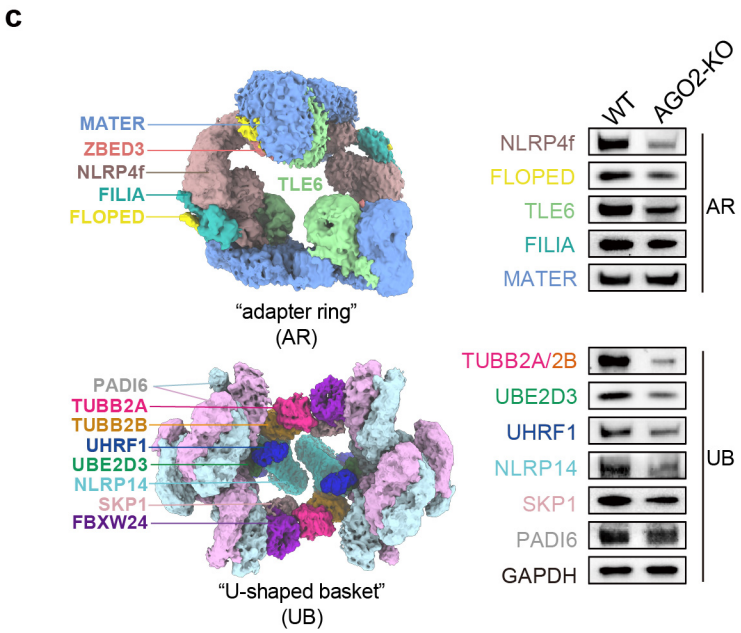

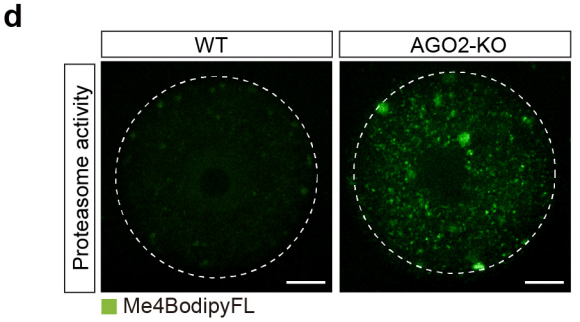

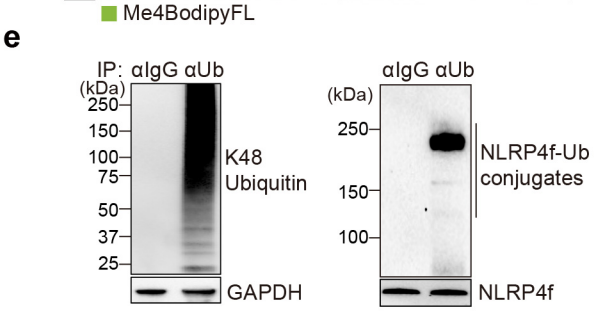

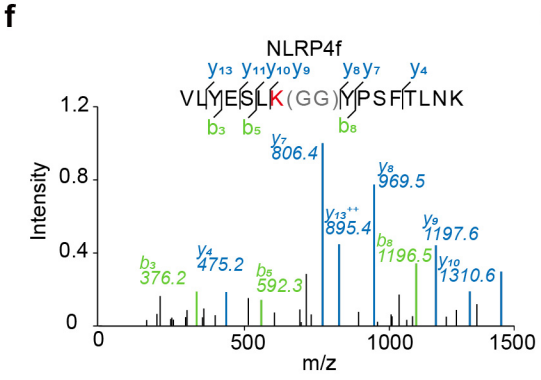

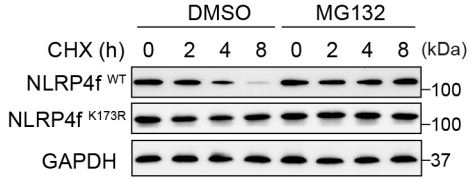

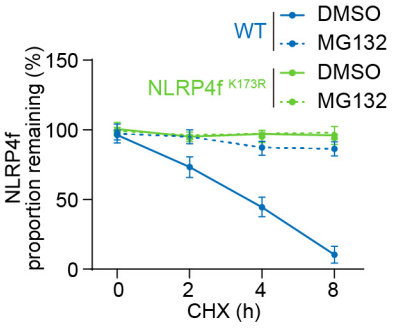

Fig. 3 AGO2 maintains CPL assembly by suppressing proteasome activity.

a, b, Representative pan-ExM images (a) and quantification (b) of wild-type and AGO2-KO mouse oocytes at different developmental stages, labeled with NHS-Atto488. Scale bars, 2.5 μm. **c**, Representative immunoblots showing expression of CPL subunits in wild-type and AGO2-KO mouse oocytes, with GAPDH as loading control. **d**, Representative micrographs of wild-type and AGO2-KO mouse oocytes stained with Me4bodiFL dye. Scale bar, 15 μm. **e,** Representative immunoblots of proteins pulled down by TUBE (Tandem ubiquitin binding entities) beads from oocyte lysates, probed with anti-NLRP4f or anti-ubiquitin antibody. IgG was used as negative control. **f,** Ubiquitination sites on NLRP4f identified by immunoprecipitation – mass spectrometry (IP – MS). **g, h,** Representative immunoblots (g) and quantification (h) of expression kinetics of wild-type and ubiquitination-site mutants of NLRP4f in HEK293F cells following cycloheximide and MG132 treatment. Data are presented as mean ± SD, with n = 3 independent experiments.

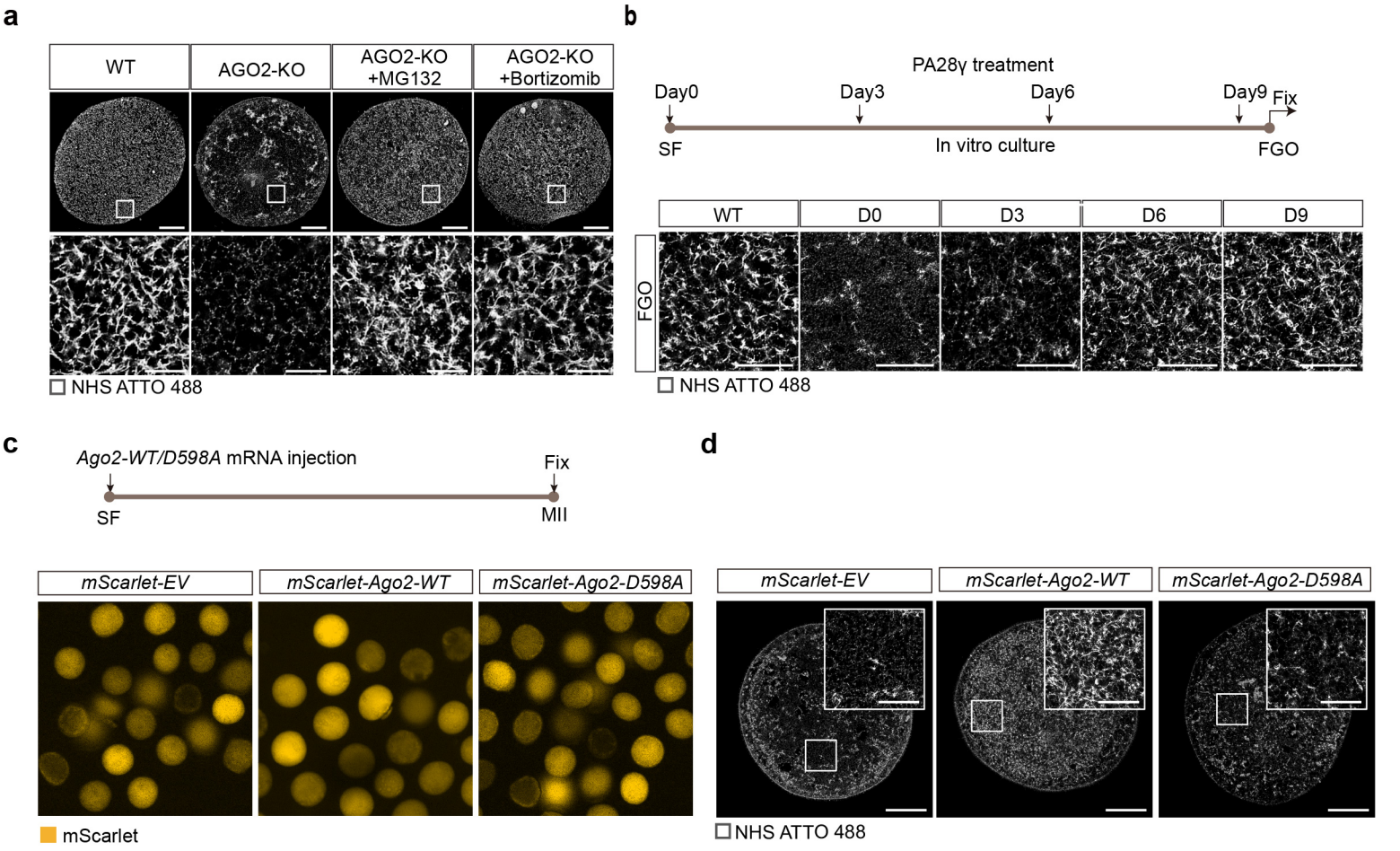

Fig. 4 CPL assembly is governed by restricted proteasome function and AGO2 slicer activity.

a, Representative pan-ExM images of wild-type and AGO2-KO mouse oocytes treated with MG132 or bortezomib, labeled with NHS-Atto488. Scale bars, 12.5 μm, scale bar of insets, 2.5 μm. **b,** Representative pan-ExM images of mouse oocytes isolated from secondary follicles (SF) and subjected to PA28γ treatment on day 0, 3, 6, or 9 of in vitro culture, followed by maturation to the fully grown oocyte (FGO) stage and labeling with NHS-Atto488. Scale bars, 2.5 μm. **c,** Representative fluorescence micrographs of oocytes microinjected with mRNAs encoding mScarlet-tagged proteins. Scale bars, 100 μm. **d,** Representative pan-ExM images of AGO2-KO mouse oocytes overexpressed with *Ago2-WT* or *Ago2-D598A* mRNA, labeled with NHS-Atto488. Scale bar, 15 μm, scale bar of insets, 5 μm.

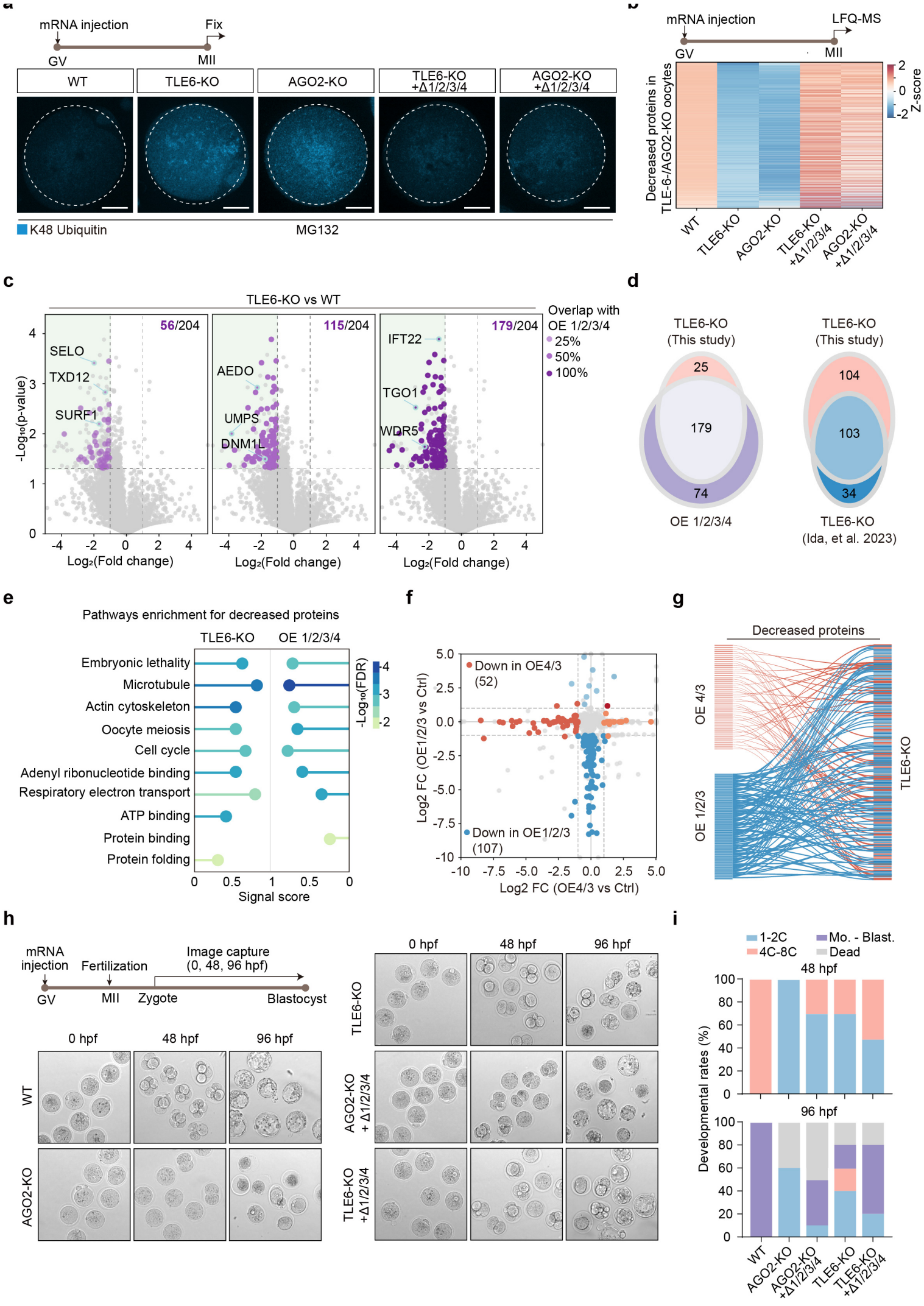

Fig. 5 CPLs shield maternal protein reservoir by sequestering ubiquitination regulators.

a, Representative immunofluorescence micrographs of wild-type, TLE6-KO, and AGO2-KO mouse oocytes, and TLE6-KO and AGO2-KO oocytes microinjected with mRNAs encoding ubiquitination-site mutants of FBXW24, SKP1, UBE2D3, and UHRF1 (Δ/1/2/3/4) immunostained for K48-linked ubiquitin. Scale bar, 15 μm. **b,** Heatmap of proteins downregulated in TLE6-KO and AGO2-KO oocytes, comparing expression across wild-type, TLE6-KO, AGO2-KO, and rescue groups expressing ubiquitination-site mutants of FBXW24, SKP1, UBE2D3, and UHRF1. Data are Z-score normalized. **c,** Volcano plot showing overlapping decreased proteins identified in TLE6 KO oocytes and under varying levels of overexpression of *Fbxw24*, *Skp1*, *Ube2d3*, and *Uhrf1* mRNAs (OE1/2/3/4). Overlapping proteins are highlighted in purple. **d,** Left, the Venn diagram shows the overlap of downregulated proteins in TLE6 KO oocytes of this study and in overexpressed *Fbxw24*, *Skp1*, *Ube2d3*, and *Uhrf1* mRNAs (OE1/2/3/4) oocytes. Right, the Venn diagram shows the overlap of decreased proteins in TLE6-KO oocytes of this study and TLE6-KO oocytes of Ida's paper. **e,** Pathway enrichment for decreased proteins in TLE6-KO oocytes and in overexpressed *Fbxw24*, *Skp1*, *Ube2d3*, and *Uhrf1* mRNAs (OE1/2/3/4) oocytes. **f,** Volcano plot showing decreased proteins in overexpressed *Ube2d3* and *Uhrf1* mRNA oocytes and in overexpressed *Fbxw24*, *Skp1,* and *Ube2d3* mRNA (OE1/2/3) oocytes, respectively. **g,** Sankey diagram shows the overlap of decreased proteins in overexpressed *Ube2d3*, and *Uhrf1* mRNA oocytes and TLE6-KO oocytes, in overexpressed *Skp1*, *Fbxw24,* and *Ube2d3* mRNA (OE1/2/3) oocytes and TLE6-KO oocytes. **h, i,** Embryo morphology (h) and developmental rates (i) derived from wildtype, AGO2-KO, and TLE6-KO oocytes, and from TLE6-KO and AGO2-KO oocytes microinjected with mRNAs encoding ubiquitination-site mutants of FBXW24, SKP1, UBE2D3 and UHRF1.

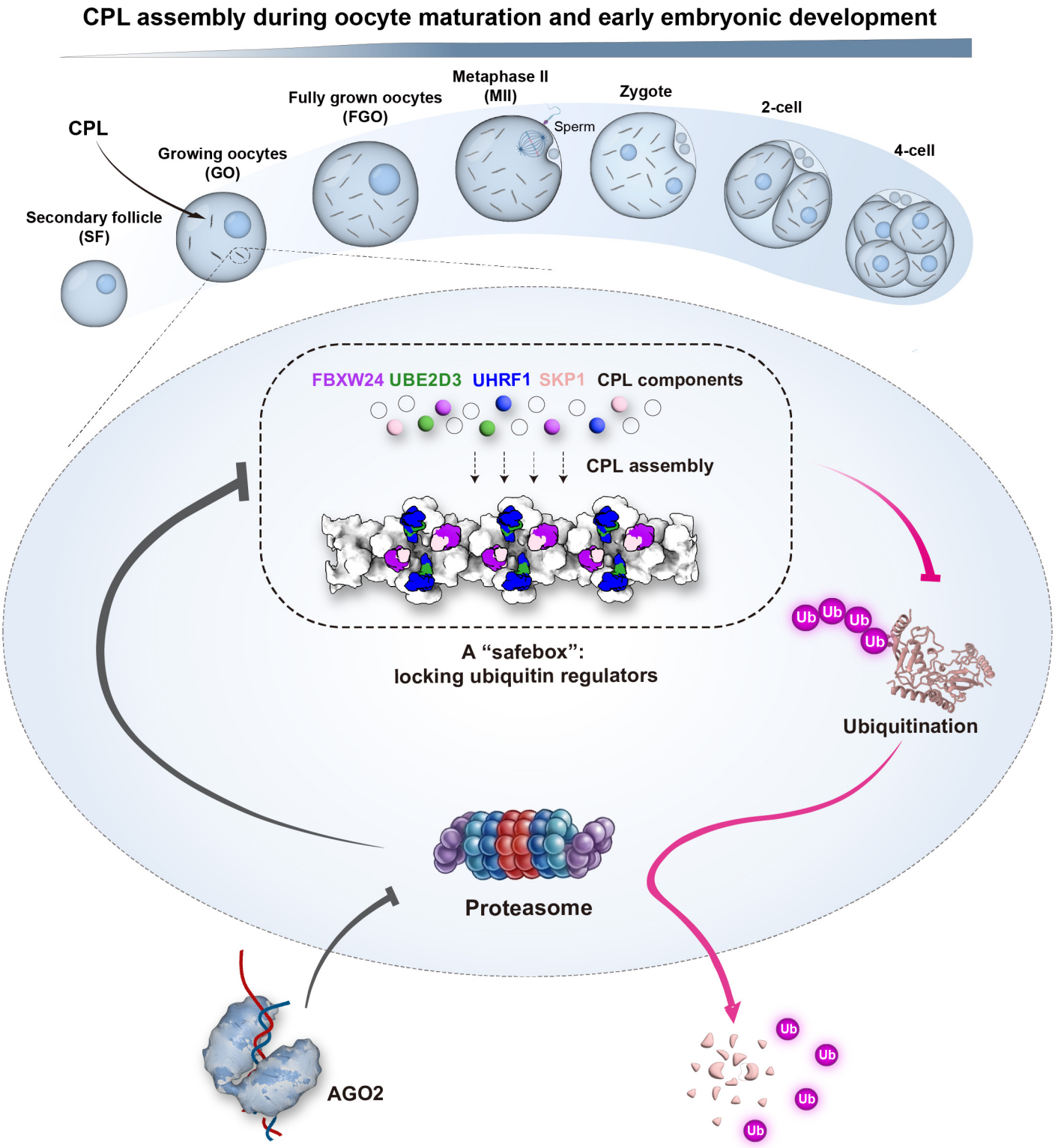

846 **Fig. 6 Model of CPL and AGO2 as a robust bistable switch in a ratchet-like cycle,**
847 **irreversibly restricting ubiquitination to preserve the maternal protein reservoir.**

848

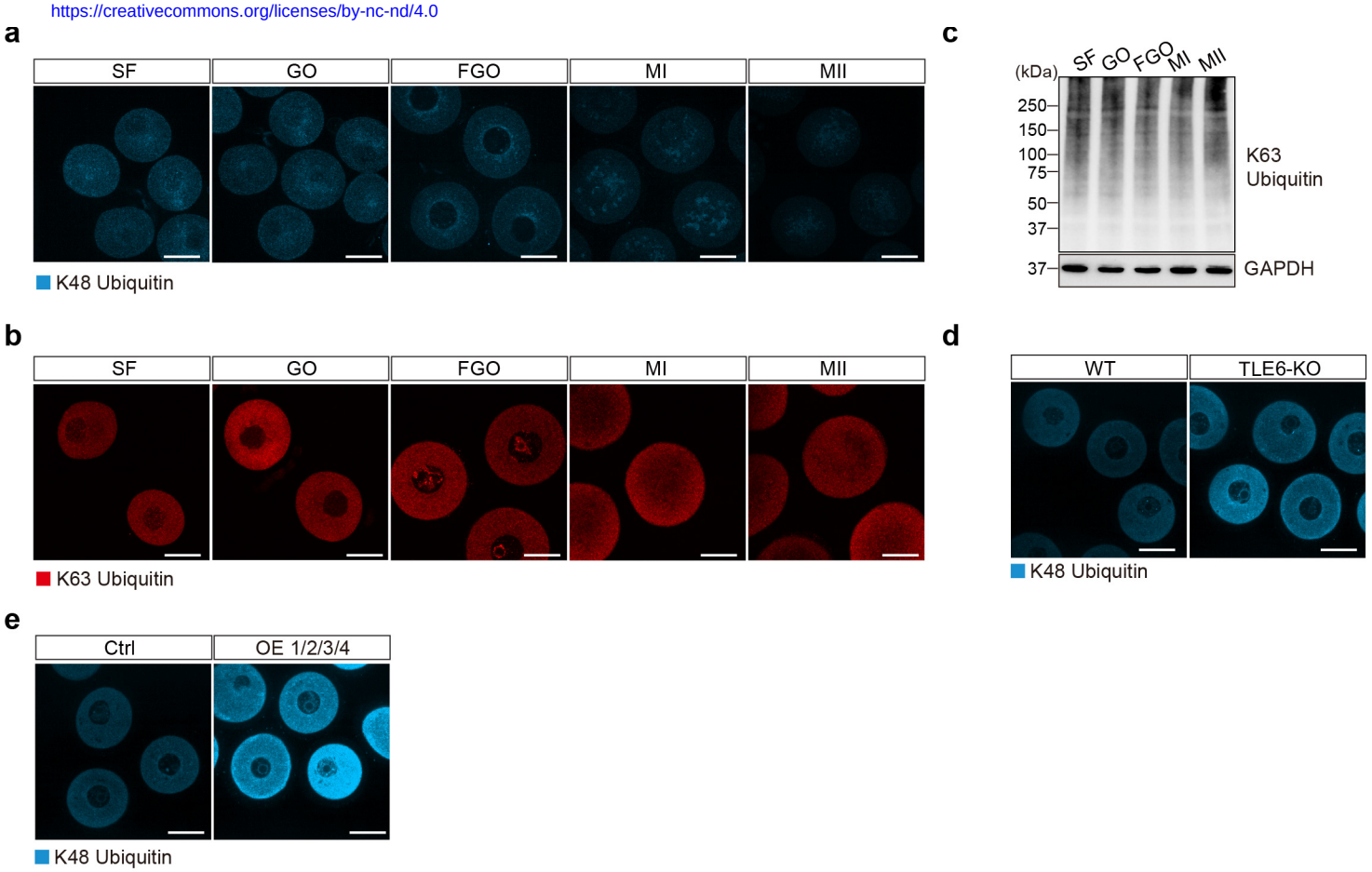

Extended Data Fig. 1 K48-linked ubiquitination and K63-linked ubiquitination in different stages of oocytes.

a, Representative micrographs of different stages of mouse wild-type oocytes stained with an anti-K48-linked ubiquitin antibody followed by a secondary antibody. Scale bar, 50 μm. **b,** Representative micrographs of different stages of mouse wild-type oocytes stained with an anti-K63-linked ubiquitin antibody followed by a secondary antibody. Scale bar, 50 μm. **c**, Representative immunoblots of lysates from wild-type mouse oocytes at different developmental stages, probed with an anti-K63-linked ubiquitin antibody. **d,** Representative micrographs of wild-type and TLE6-KO mouse oocytes stained with an anti-K48-linked ubiquitin antibody. Scale bar, 50 μm. **e,** Representative micrographs of wild-type mouse oocytes microinjected with a mixture of *Fbxw24*, *Skp1*, *Ube2d3*, and *Uhrf1* mRNAs (OE1/2/3/4) and stained with an anti-K48-linked ubiquitin antibody. Scale bar, 50 μm.

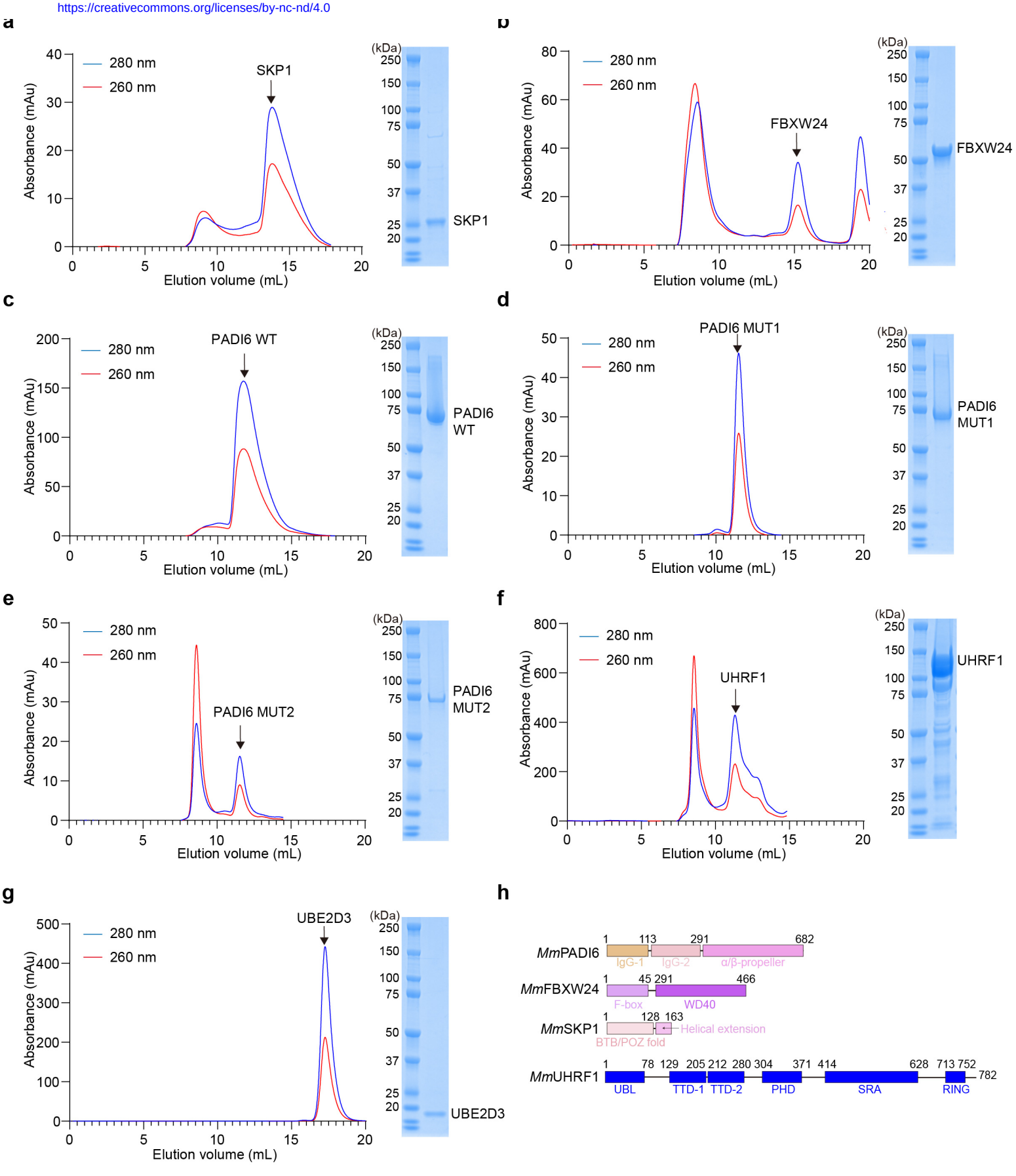

Extended Data Fig. 2 Proteins purified in this study.

a, Size-exclusion chromatography profile and SDS-PAGE analysis of the purified Flag-SKP1 protein. **b**, Size-exclusion chromatography profile and SDS-PAGE analysis of the purified FBXW24-Flag protein. **c,** Size-exclusion chromatography profile and SDS-PAGE analysis of the purified Flag-PADI6-WT protein. **d,** Size-exclusion chromatography profile and SDS-PAGE analysis of the purified Flag-PADI6-Mutant1 protein. **e,** Size-exclusion chromatography profile and SDS-PAGE analysis of the purified HIS-MBP-UHRF1 protein. **f,** Size-exclusion chromatography profile and SDS-PAGE analysis of the purified HIS-UBE2D3 protein. **g,** Size-exclusion chromatography profile and SDS-PAGE analysis of the purified Flag-PADI6-Mutant2 protein. **h,** Domain organizations of *Mm*PADI6*, Mm*FBXW24*, Mm*SKP1 *and Mm*UHRF1, the domain boundary is labeled. **i,** Pull-down assay of purified proteins assessing the effects of PADI6 $^{N158A,\ Q162A,\ R173A}$ on the interaction of FBXW24 and SKP1. **j,** Pull-down assay of purified proteins assessing the effects of PADI6 $^{K333A,\ E336A,\ Q341A,\ Y380A,\ N586A,\ D653A,\ N658A,\ D661A}$ on the interaction of UBE2D3 and UHRF1.

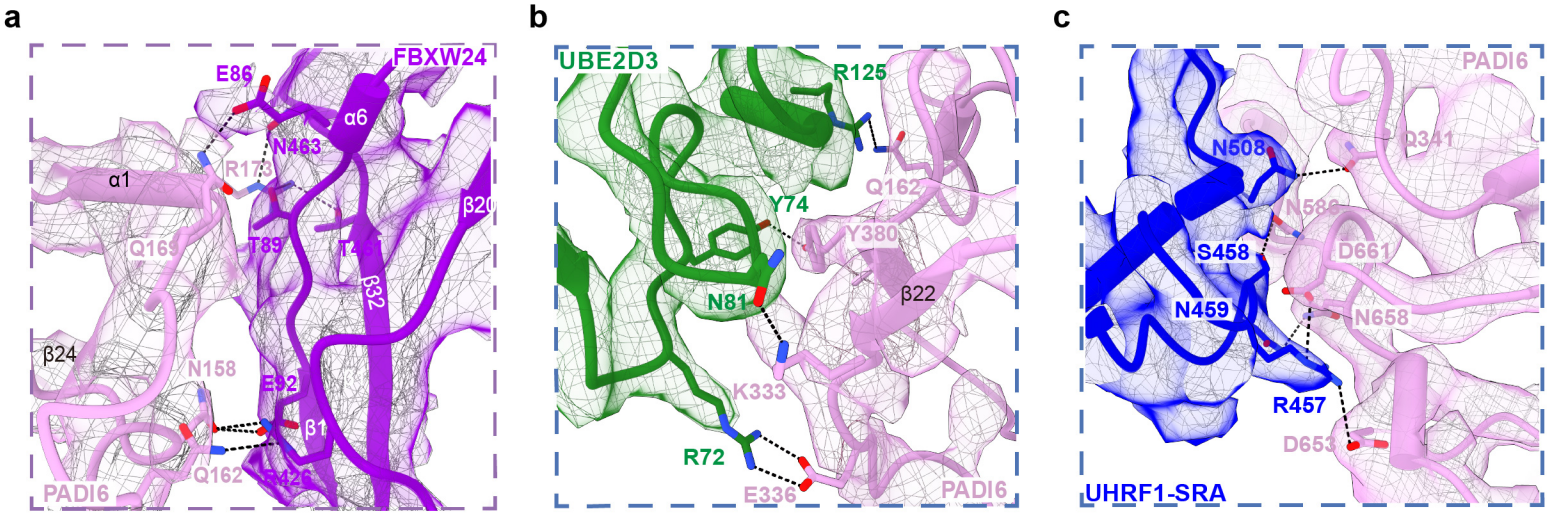

877 **Extended Data Fig. 3 Structure details of PADI6 and ubiquitination regulators**

878 **a,** Interactions between PADI6 and FBXW24. **b,** Interactions between PADI6 and UBE2D3. **c,**

879 Interactions between PADI6 and UHRF1.

880

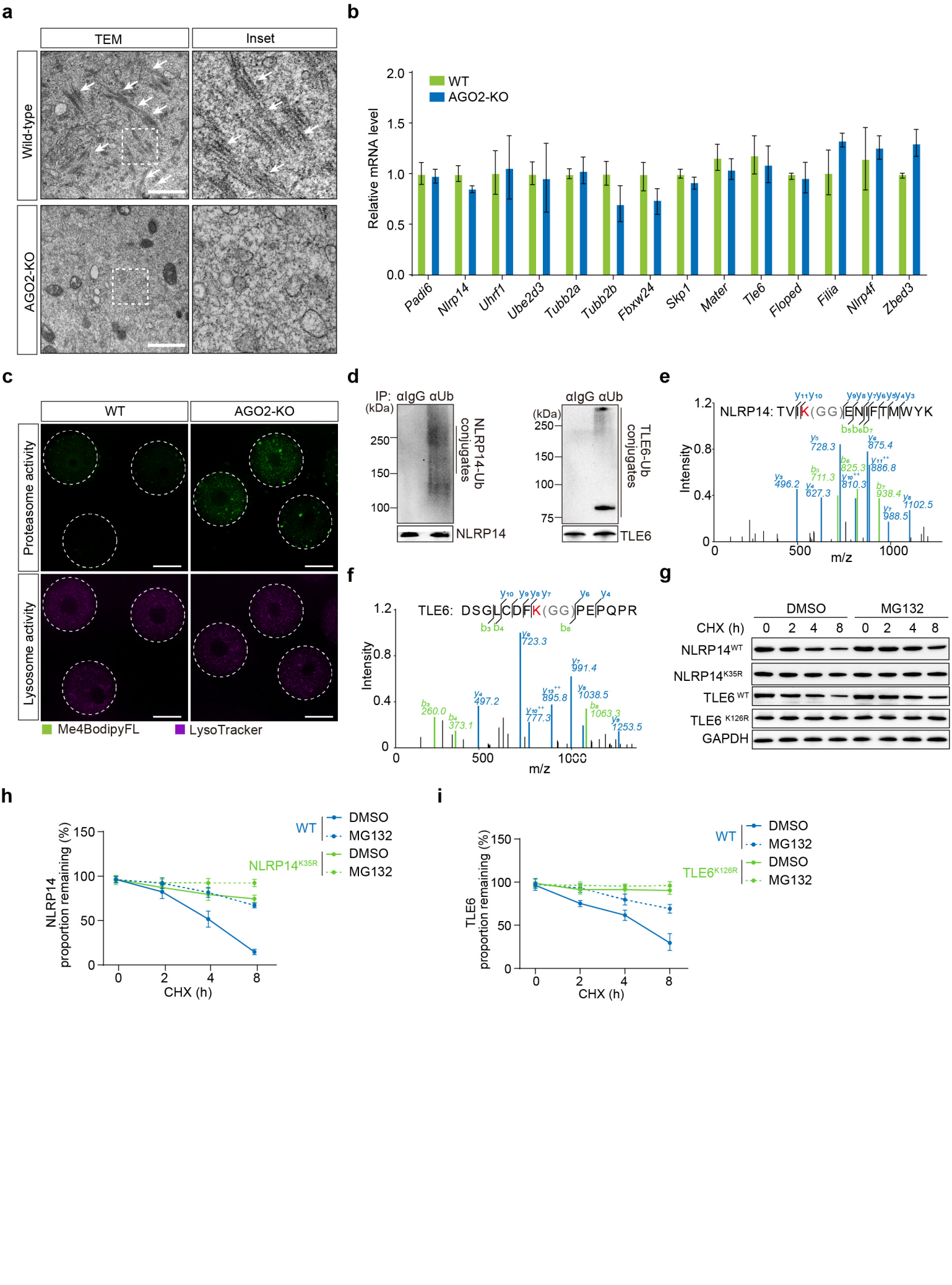

Extended Data Fig. 4 AGO2 regulate proteasome activity to safeguard CPL integrity.

a, Representative TEM images of CPL in wild-type and AGO2 KO mouse oocytes. Scale bars, 500 nm. **b**, qPCR results of the expression levels of 14 CPL subunits in wild-type and AGO2-KO mouse oocytes. Data are presented as mean ± SD, with n = 3 independent experiments. **c**, Representative micrographs of wild-type and AGO2-KO mouse oocytes stained with Me4bodiFL dye and Lyso Tracker. Scale bar, 50 μm. **d**, Representative immunoblots of proteins pulled down by TUBE (Tandem ubiquitin binding entities) beads from oocyte lysates, probed with anti-NLRP14 and anti-TLE6 antibodies. IgG was used as negative control. **e, f,** Ubiquitination sites on NLRP14 and TLE6 identified by immunoprecipitation – mass spectrometry (IP–MS). **g,** Representative immunoblots of wild-type and ubiquitination-site mutants of NLRP14 and TLE6 in HEK293F cells following cycloheximide and MG132 treatment. **h, i,** Representative quantification of expression kinetics of wild-type and ubiquitination-site mutants of NLRP14 and TLE6 in HEK293F cells following cycloheximide and MG132 treatment.

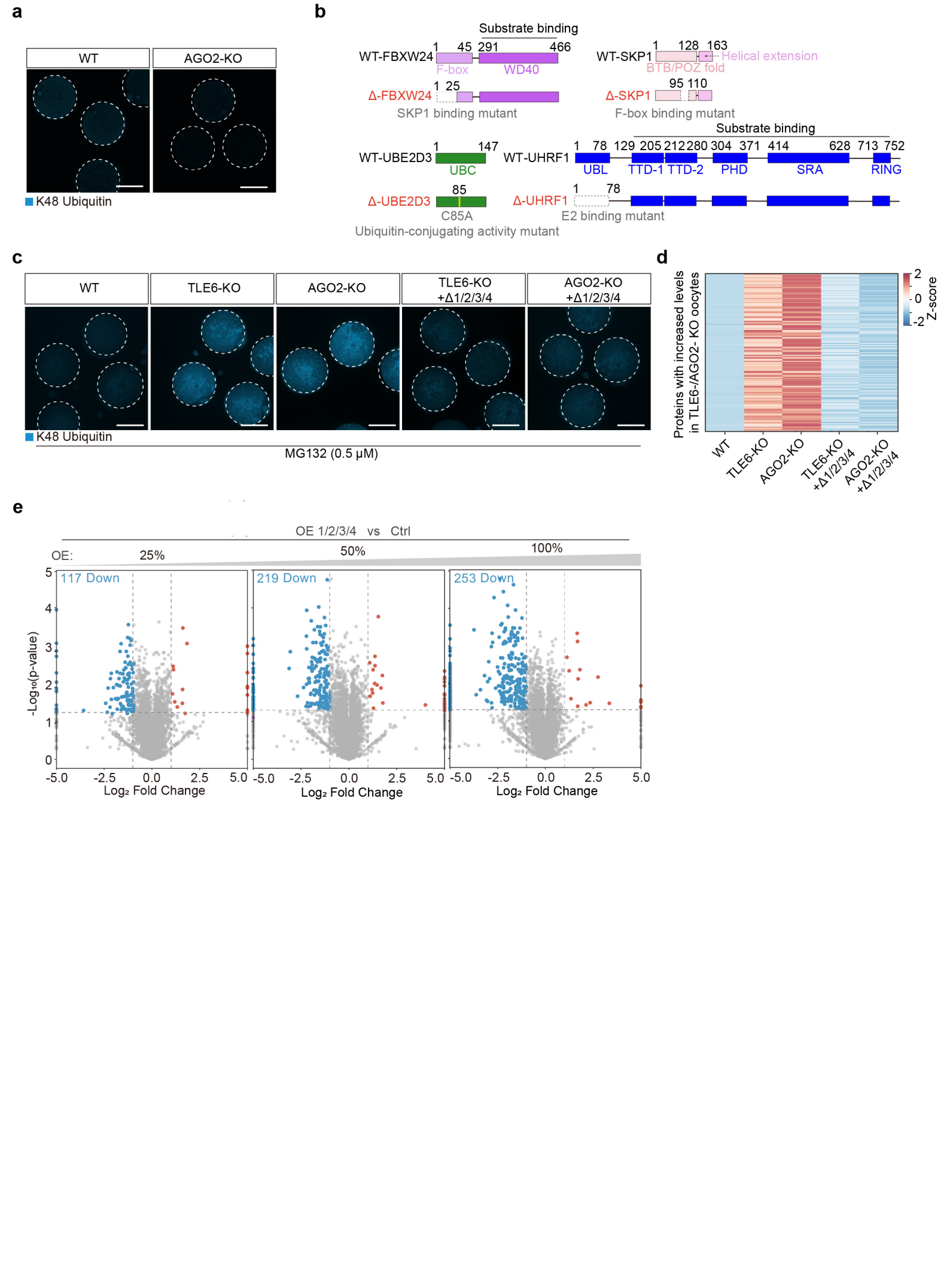

Extended Data Fig. 5 Overexpression of ubiquitination regulator mutants decreases ubiquitination and perturbs the homeostasis of maternal proteins.

a, Representative micrographs of wild-type and AGO2-KO mouse oocytes stained with an anti-K48-linked ubiquitin antibody. Scale bar, 50 μm. **b,** Domain organizations of *Mm*FBXW24 and its mutant, *Mm*UHRF1 and its mutant, the domain boundary is labeled. **c,** Representative immunofluorescence micrographs of wild-type, TLE6-KO, and AGO2-KO mouse oocytes, and TLE6-KO and AGO2-KO oocytes microinjected with mRNAs encoding ubiquitination-site mutants of SKP1, FBXW24, UHRF1, and UBE2D3, immunostained for K48-linked ubiquitin. Scale bars, 50 μm. **d,** Heatmap of proteins upregulated in TLE6-KO and AGO2-KO oocytes, comparing expression across wild-type, TLE6-KO, AGO2-KO, and rescue groups expressing ubiquitination-site mutants of SKP1, FBXW24, UHRF1, and UBE2D3. Data are Z-score normalized. **e,** Volcano plot showing downregulated proteins identified in oocytes following graded overexpression of *Fbxw24*, *Skp1*, *Ube2d3*, and *Uhrf1* mRNAs (OE1/2/3/4).

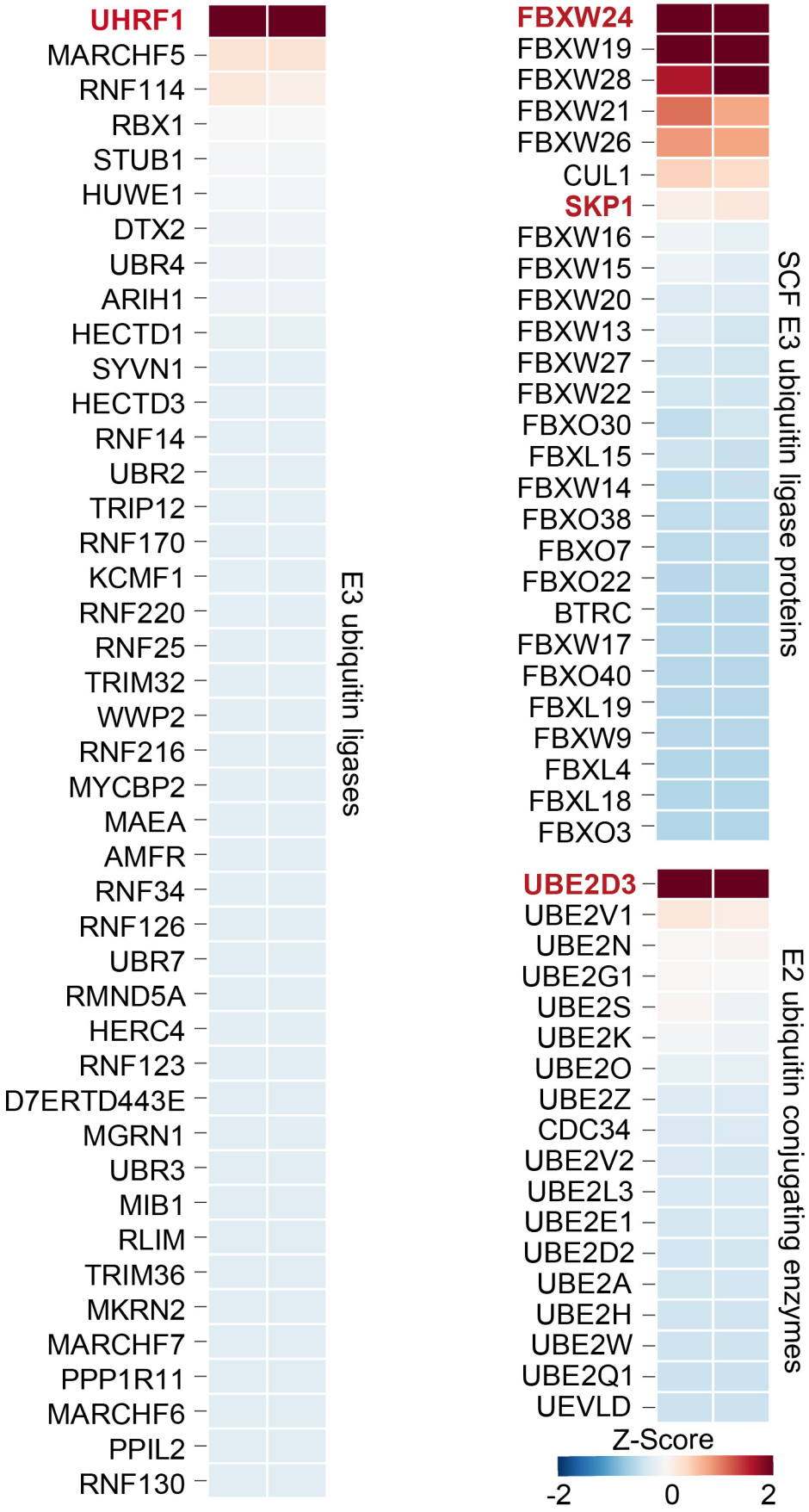

Extended Data Fig. 6 Expression levels of ubiquitination regulators in oocytes.

Heatmap showing the relative expression levels of SCF type E3 ubiquitin ligases, other E3 ubiquitin ligases and E2 ubiquitin-conjugating enzymes in oocytes.

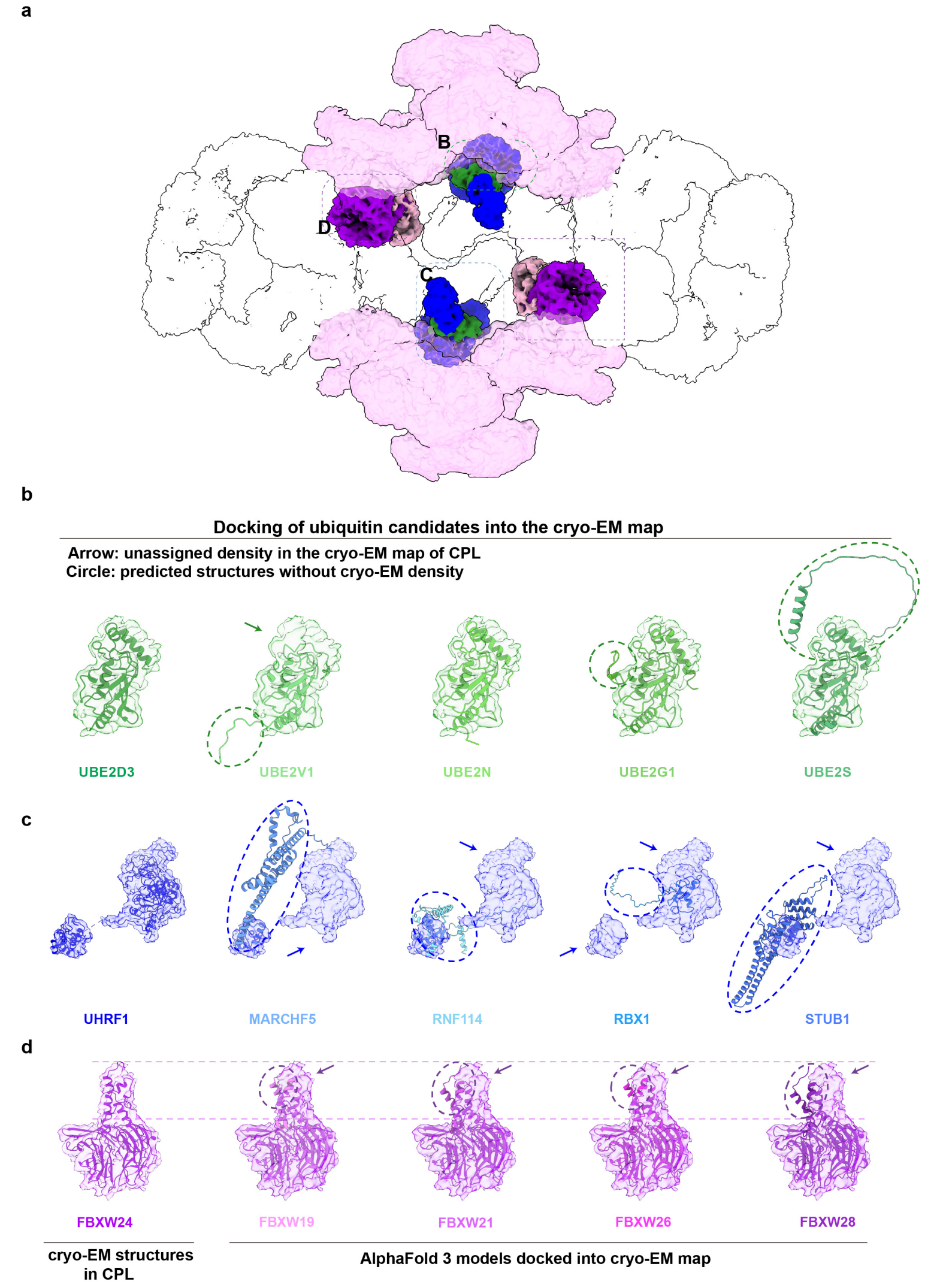

913 **Extended Data Fig. 7 CPL specifically incorporates ubiquitination regulators.**

914 **a,** The spatial arrangement of UBE2D3, UHRF1, and FBXW24 in CPL. **b, c, d,** Structural
915 analysis of highly expressed E2 ubiquitin-conjugating enzymes, E3 ubiquitin ligases, and F-
916 box proteins.

917